Forschungszentrum Karlsruhe
Technik und Umwelt

Wissenschaftliche Berichte
FZKA 6706

Long-Term Performance of Candidate Materials for HLW/Spent Fuel Disposal Containers

E. Smailos, M. Á. Cuñado, I. Azkarate, B. Kursten, G. Marx

Institut für Nukleare Entsorgung

Februar 2002

FORSCHUNGSZENTRUM KARLSRUHE
Technik und Umwelt

Wissenschaftliche Berichte
FZKA 6706

Long-Term Performance of Candidate Materials for HLW/Spent Fuel Disposal Containers

1. Annual Progress Report (November 2000 - October 2001)

E. Smailos, M.Á. Cuñado[1)], I. Azkarate[2)], B. Kursten[3)], G. Marx[4)]

Institut für Nukleare Entsorgung

[1)] ENRESA,Spain
[2)] INASMET, Spain
[3)] SCK.CEN, Belgium
[4)] GNF.IUT, Germany

EC-Contract No. FIKW-CT-2000-00004

Forschungszentrum Karlsruhe GmbH, Karlsruhe
2002

ACKNOWLEDGEMENT

The work was performed within the 5th EURATOM FRAMEWORK PROGRAMME 1998-2002, Key Action: NUCLEAR FISSION.

The authors thank the European Commission in Brussels, Belgium for funding of this project.

Forschungszentrum Karlsruhe GmbH
Postfach 3640, 76021 Karlsruhe

Mitglied der Hermann von Helmholtz-Gemeinschaft
Deutscher Forschungszentren (HGF)

ISSN 0947-8620

EXECUTIVE SUMMARY

In the project "Corrosion Evaluation of Metallic Materials for Long-Lived HLW/Spent Fuel Disposal Containers," in-depth corrosion studies are performed on preselected container materials in rock salt, granite and clay environments. The materials investigated are carbon steel, stainless steels, Ni-base alloys (Hastelloy C-4 and Hastelloy C-22), the alloy Ti99.8-Pd and Cu-base materials. The objectives of the studies are: to determine the influence of essential parameters (e.g., composition of the medium, temperature etc.) on corrosion, to gain a better understanding of corrosion mechanisms, and provide more accurate data for modeling the corrosion of the containers over hundred of years.

To achieve the objectives of the project, a combination of chemical experiments (long-term immersion tests), electrochemical studies, and stress corrosion cracking studies are performed. The project is a joint undertaken of FZK.INE (project co-ordinator; investigations in rock salt and granite), GNF.IUT (investigations in rock salt), ENRESA/INASMET (studies in granite), and SCK.CEN (studies in clay).

The project started on 1 November 2000 and will last three years till 31 October 2003. In the present paper the results of the investigations performed during the first year of the project are presented.

The results of the investigations in $MgCl_2$-rich brine (T = 150°C) indicate that the welded specimens of the TStE355 carbon steel suffer from severe pitting corrosion. However, the stress relief thermal treated welds are resistant to pitting corrosion, as do so the unwelded specimens. In NaCl-rich brine, the welded steel is resistant to pitting corrosion and suffers only from general corrosion as the unwelded material. Investigations on contact specimens of the material pair Ti99.8-Pd and TStE355 steel in NaCl-rich brine at 150°C show that the coupling of these materials does not cause contact corrosion. Cu, Ni and Cu-Ni alloys (90-10 and 70-30) have between 25°C and 80°C in salt brines a large passive range, and the corrosion rates are low (8 - 30 µm/a).

Potentiodynamic polarization tests (20°C) in granitic-bentonite water show that Hastelloy C-22, Cu-OF and Cu-Ni 70-30 are resistant to pitting corrosion. Furthermore, Hastelloy C-22 is resistant to crevice corrosion (Cl^--content: 50,000 mg/l) and to stress corrosion cracking in granitic-bentonite water. Cu-OF shows a slight crevice corrosion in this medium.

In clay water (anaerobic conditions) at 16°C and a Cl^- content up to 50,000 mg/l, the materials Ti99.8-Pd, Hastelloy C-4, Hastelloy C-22 and the stainless steel UHB 904L are resistant to pitting corrosion. The stainless steels AISI 316L and AISI 316Ti show pitting corrosion at Cl^--concentrations higher than 20,000 mg/l. At the higher temperature of 90°C, only Ti99.8-Pd remains resistant to general and pitting corrosion. The carbon steel TStE355 exhibits general corrosion, and the susceptibility of UHB 904L to pitting corrosion increases with growing Cl^--content. However, no serious corrosion problems are expected for the UHB 904L steel under realistic disposal conditions in clay. The alloys Hastelloy C-4 and Hastelloy C-22 suffer from pitting only in solutions containing more than 20,000 mg/l Cl^-. At 140°C and aerobic conditions in clay water, the susceptibility of the UHB 904L steel to pitting is higher than at 90°C.

KORROSIONSBESTÄNDIGKEIT AUSGEWÄHLTER BEHÄLTERWERKSTOFFE FÜR DIE ENDLAGERUNG VON HOCHRADIOAKTIVEN ABFÄLLEN UND ABGEBRANNTEN BRENNELEMENTEN

ZUSAMMENFASSUNG

Im Rahmen des EU-Projektes „Long-term performance of candidate materials for HLW/Spent fuel disposal containers" wird das Korrosionsverhalten ausgewählter metallischer Werkstoffe unter simulierten Endlagerbedingungen in Steinsalz, Granit und Ton untersucht. Die untersuchten Werkstoffe sind ein unlegierter Stahl, legierte Cr-Ni-Stähle, Nickelbasislegierungen (Hastelloy C4 und Hastelloy C12), die Legierung Ti99,8-Pd und Kupferbasiswerkstoffe (Cu und Cu-Ni-Legierungen). Die Ziele der Untersuchungen sind: Bestimmung des Einflusses wichtiger Parameter auf das Korrosionsverhalten der Werkstoffe, Verbesserung der Kenntnisse über die Korrosionsmechanismen und die Gewinnung von sicheren Daten für ein Korrosionsmodell, mit dem die Standzeit der Behälter unter Endlagerbedingungen prognostiziert werden kann.

Die Untersuchungen umfassen chemische Experimente (Langzeit-Immersionstests), elektrochemische Untersuchungen und Spannungsrißkorrosionsuntersuchungen. Das Projekt ist ein gemeinsames Vorhaben von FZK.INE (Projektkoordinator, Untersuchungen in Steinsalz und Granit), GNF.INT (Untersuchungen in Steinsalz), ENRESA/INASMET (Untersuchungen in Granit) und SCK.CEN (Untersuchungen in Ton). Das Projekt dauert drei Jahre (November 2000 – Oktober 2003). In der vorliegenden Arbeit wird über die im ersten Projektjahr gewonnenen Untersuchungsergebnisse berichtet.

Die Untersuchungsergebnisse an dem unlegierten Feinkornbaustahl TStE355 in $MgCl_2$-reicher Lösung (T=150°C) zeigen, daß die nicht wärmebehandelten Schweißproben stark anfällig gegenüber Lochkorrosion sind. Die spannungsfrei geglühten geschweißten Stahlproben hingegen sind so beständig gegenüber Lochkorrosion wie die ungeschweißten Proben. In NaCl-reicher Lösung ist der geschweißte Stahl mit und ohne Wärmebehandlung der Schweißnähte beständig gegen Lochkorrosion. Bei den Untersuchungen am Werkstoffpaar Ti99,8-Pd/TStE355 in NaCl-reicher Lösung war keine Kontaktkorrosion festzustellen. Die Werkstoffe Cu, Ni und deren Legierungen Cu-Ni 90-10 und Cu-Ni 70-30 haben in Salzlösungen zwischen 25°C und 80°C einen breiten passiven Bereich und deren Korrosionsraten sind niedrig (8-30 µm/a).

In Granitwasser (T=90°C) sind Hastelloy C22, Cu und Cu-Ni 70-30 beständig gegenüber Lochkorrosion. Darüber hinaus zeigt in diesem Medium die Legierung Hastelloy C22 eine gute Beständigkeit gegenüber Spaltkorrosion (Cl^-: 50.000 mg/l) und Spannungsrißkorrosion, während Cu leicht empfindlich gegenüber Spaltkorrosion ist.

In Tonwasser (anaerobe Bedingungen) bei 16°C und einem Cl^- Gehalt von 50.000 mg/l sind die Werkstoffe Ti99,8-Pd, Hastelloy C4, Hastelloy C22 und der Cr-Ni Stahl UHB 904 L beständig gegenüber Lochkorrosion. Die Cr-Ni Stähle AISI 316 L und AISI 316 Ti zeigen bei Cl^-Konzentrationen höher als 20.000mg/l Lochkorrosion. Bei der höheren Temperatur von 90°C ist nur die Legierung Ti99,8-Pd beständig gegenüber Flächen- und Lochkorrosion. Bei dem unlegierten Stahl TStE 355 ist eine Flächenkorrosion und bei dem Cr-Ni Stahl UHB 904L eine zunehmende Empfindlichkeit gegenüber Lochkorrosion mit steigendem Cl^- Gehalt festzustellen. Allerdings sind bei dem Stahl UHB 904 L bei realistischen Cl^- Gehalten in Ton keine ernsthaften Korrosionsprobleme zu erwarten. Die Legierungen Hastelloy C4 und Hastelloy C22 erweisen sich als empfindlich gegenüber Lochkorrosion nur in Tonwässern mit einem Cl^- Gehalt höher als 20.000 mg/l. Bei 140°C und aeroben Bedingungen in Tonwasser ist die Empfindlichkeit des Stahls UHB 904 L gegenüber Lochkorrosion deutlich höher als bei 90°C.

TABLE OF CONTENTS

		Page
	EXECUTIVE SUMMARY	
1.	**OBJECTIVES AND EXPECTED OUTCOME**	1
2.	**SCIENTIFIC AND TECHNICAL PERFORMANCE**	2
2.1	Corrosion studies in salt environments	2
2.1.1	Influence of welding and heat treatment on corrosion of the TStE355 carbon steel in salt brines	2
2.1.2	Contact corrosion between TStE355 carbon steel and Ti99.8-Pd in NaCl-rich brine	5
2.1.3	Electrochemical studies on Copper, Nickel and Copper-Nickel alloys	7
2.2	Corrosion studies in granitic-bentonite environment	9
2.2.1	Stress corrosion cracking studies	10
2.2.2	Electrochemical corrosion studies	10
2.2.3	Crevice Corrosion studies	11
2.3	Corrosion studies in clay environments	12
2.3.1	Materials and experimental techniques	12
2.3.2	Results	14
3.	**CONCLUSIONS**	16
4.	**REFERENCES**	17
5.	**MANAGEMENT AND CO-ORDINATION ASPECTS**	18
6.	**DEPARTURES FROM THE WORK PLAN**	18
7.	**PLANNED ACTIVITIES FOR THE NEXT REPORTING PERIOD**	19
8.	**LIST OF DISTRIBUTED PAPERS**	20
	Tables 1-13	21-26
	Figures 1-31	27-40
	ANNEX: Updated time schedule of the project	

1. OBJECTIVES AND EXPECTED OUTCOME

In present concepts for the disposal of vitrified high-level waste (HLW) and spent fuel in geological formations such as rock salt, granite and clay, the disposal container is one of several barriers against the mobilization of radionuclides. The main threat to container integrity is corrosion induced by contact with salt brines or groundwater which may be present in the disposal area under certain conditions. Accordingly, extended studies have been undertaken in various EU-laboratories aimed at identifying corrosion resistant materials for long-lived containers.

Previous corrosion studies in the frame of EC-Projects yielded a considerable amount of information on the corrosion behaviour of various materials such as carbon steel, stainless steels, nickel- and titanium alloys under disposal conditions. A large number of experimental data was gained which should be used for the development of materials degradation models in order to predict the lifetime of the containers. From the results obtained in previous studies [1,2,3,4,5], the following conclusions can be drawn:

- The passively corroded alloy Ti99.8-Pd is the strongest candidate for the corrosion-resistant container concept in rock salt, granite and clay.

- The actively corroded carbon steel is the most promising material for the corrosion allowance container concept in the above-mentioned geological formations. However, its general corrosion rate at high temperature (150°C) in $MgCl_2$-rich brines is very high, which leads to very thick-walled containers and to undesirable high amounts of H_2 in the repository. Therefore, alternative materials such as Cu-base materials will be investigated.

- Hastelloy and high alloyed stainless steels seem to be potential container materials for disposal in clay at realistic Cl^- concentrations.

The objectives of the present corrosion programme are:

- A reliable assessment of the suitability of the above-mentioned candidate container materials in the various repositories by examination of the influence of important parameters on the corrosion behaviour, and clarification of essential questions remaining from the previous EC-project.
- To evaluate the suitability of potential alternative container materials.
- To achieve a better understanding of the corrosion mechanisms and to provide the necessary data for modeling the corrosion of the containers over hundreds of years.

To achieve the objectives of the project a combination of chemical experiments (long-term immersion tests), electrochemical studies and stress corrosion cracking studies will be performed in the EU-partners´ laboratories.

Essential aspects of the studies in salt environments are to investigate the contact corrosion between Ti99.8-Pd (outer container) and carbon steel (inner container) and to

examine the influence of welding (simulation of a container closure technique) and thermal stress relief treatment of the welds on the corrosion behaviour of carbon steel.

Further important points are the evaluation of copper and copper alloys as container materials (alternative materials for carbon steel) and the examination of the influence of gamma radiation on the corrosion of the various materials. In granitic-bentonite environment, the corrosion behaviour of various materials (steel, copper-base, and nickel-base materials) to general and local corrosion and stress corrosion cracking will be investigated. In clay/bentonite environment, the influence of various parameters (anaerobic conditions, elevated temperature and radiolysis products) on the corrosion of carbon steel, stainless steels, Hastelloy C4 and C22, and Ti99.8-Pd will be studied.

The corrosion results can be used to develop materials degradation models in order to predict the lifetime of the containers over hundred of years. A container corrosion model can be combined with other models (e.g. spent fuel and HLW glass models) to describe the source term in the near field in the framework of safety analyses for a repository.

The results will be disseminated to organizations responsible for implementing the programmes for disposal of radioactive waste and will be published in accordance with the rules set up by the European Commission. Since all partners are involved in research into repository safety, the participating organizations will be also end-users of the results.

The results of the project could be used in all European Union countries as the project is independent of the type of fuel cycle of HLW waste (spent fuel or glass) and the characteristics of the host rock environment.

In the present report, the progress achieved in the research programme from November 2000 to October 2001 shall be described.

2. SCIENTIFIC AND TECHNICAL PERFORMANCE

2.1 Corrosion studies in salt environments (WP1) (FZK.INE, GNF.IUT)

2.1.1 Influence of welding and heat treatment on corrosion of the TStE355 carbon steel in disposal relevant salt brines (WP1.1) (FZK.INE)

Welding techniques such as Electron Beam welding (EB-welding) and Tungsten Inert Gas welding (TIG-welding) are considered as potential closure techniques for carbon steel containers.

To ensure the desired lifetime of the containers, the welded container cover should have a corrosion resistance similar to that of the parent material. Under this aspect, comparative corrosion investigations on unwelded (parent material) and TIG- and EB-welded steel specimens were performed in this study. The investigation of welds is important because welding causes changes in the material structure and generates tensile stresses in the weld region and in the Heat Affected Zone (HAZ), which in turn can cause an unfavourable corrosion behaviour of the welded material.

Steel investigated and experimental

The preselected carbon steel TStE355 was investigated in the hot-rolled and annealed condition and had the following composition in wt.%: 0.17% C; 0.44% Si; 1.49% Mn; bal. Fe.

For the investigations, flat specimens having the dimensions 40mmx20mmx4mm were used. The steel was examined in three material conditions:

- Unwelded (parent material).
- Only-welded (EB- and TIG-welded).
- Welded and thermal treated. These specimens were welded by EB and TIG, and subsequently stress-relief thermal treated for 2 hours at 600°C.

In the case of the welded specimens, the weld was located in the center of the specimens in the transverse direction.

The steel specimens were examined up to 16 months in two disposal-relevant brines at the realistic disposal temperature of 150°C.The brines had at 55°C the following compositions in wt.%.:

– $MgCl_2$-rich "Q-brine" (brine 1): 26.8 $MgCl_2$; 4.7 KCl; 1.4 NaCl; 1.4 $MgSO_4$; 65.7 H_2O (pH = 4.6).
– NaCl-rich brine (brine 3): 25.9 NaCl; 0.23 K_2SO_4; 0.21 $CaSO_4$; 0.16 $MgSO_4$; 73.5 H_2O (pH = 6.5).

The experiments in Q-brine were performed in the present of a gamma radiation field of 10 Gy/h, which is relevant for the thick-walled containers discussed. The experiments in NaCl-rich brine were conducted without gamma radiation because previous investigations [6] have shown that in this brine the gamma radiation of 10 Gy/h does not affect the corrosion behaviour of the steel.

The experimental setups used for the experiments are described in previous work [5]. Briefly, for the experiments without irradiation, stainless steel pressure vessels provided with corrosion resistant insert vessels made of PTFE were used to avoid evaporation of the brines (boiling point: about 115°C). The experiments under gamma irradiation were performed in the spent fuel storage pool of KFA Jülich. For these experiments, autoclaves made of Ti99.8-Pd were used. With these experimental equipments, the initial test conditions were oxidizing. The total amount of oxygen available in the systems was about 15 mg, corresponding to 0.19 mg O_2/cm^2 specimen. This oxygen amount was consumed very fast by reactions with Fe so that after a few days reducing conditions were established. Evaluation of the specimens regarding general and local corrosion was carried out by gravimetry, measurements of pit depth, surface profilometry and metallography. The integral corrosion rate of the specimens was calculated from the experimental determined weight losses and the material density.

Results in the $MgCl_2$-rich brine "Q-brine"

Figure 1 shows the time-dependence of the general corrosion, expressed as the integral thickness reduction, of the unwelded and only-welded steel specimens in the Q-brine at 150°C and 10 Gy/h. The data indicate that the thickness reduction of the specimens increases linearly with the exposure time in the brine over the test duration of the study. The integral thickness reduction of the welded specimens is lower than that of the unwelded specimens. This is attributed to the formation of a dense layer on the specimens surface after welding which was observed in the metallographic examinations. However, the slope of the curves indicates that the linear thickness reduction of the only-welded specimens, which is the basis for the determination of the long-term corrosion rate, is very close to that of the unwelded specimens.

The linear corrosion rates of the unwelded and only-welded specimens, calculated from the slope of the curves, are compiled in Table 1. In this Table the results of the local corrosion of the specimens are also summarized, which were obtained from the surface profilometry and the metallographic examinations. The Table 1 shows that the linear corrosion rates of the only-welded specimens (66-68 µm/a) are very close to the value of the unwelded specimens (73 µm/a). For the unwelded specimens, a non-uniform general corrosion with a maximum depth of only 60 µm after 550 days was observed. In the case of the EB- and TIG- welded specimens, however, severe local corrosion attacks occurred in the weld region and in the HAZ with maximum pit depths of about 1350-1500 µm after 300 days test time.

Generally, it can be stated that the EB- and TIG-welded specimens have a very similar corrosion behaviour in the brine, and that they exhibit a significantly lower corrosion resistance than the base material.

The general corrosion and local corrosion results obtained for the thermal treated welded steel specimens in Q-brine at 150°C and 10 Gy/h are given in Figure 2 and Table 2. For comparison, the results obtained on unwelded and only-welded specimens are also given. The thickness reduction of the thermal treated welded specimens increases linearly with the exposure time in the brine (Figure 2), as do so also unwelded and only-welded specimens.

The linear corrosion rates (Table 2) of the thermal treated EB- and TIG-welded specimens (95 µm/a – 112 µm/a) are higher than the values of the unwelded (73 µm/a) and only welded specimens (66-68 µm/a). However, a such increase is not significant for the thick-walled containers discussed. Very important is the fact that corrosion of the thermal treated welded specimens is only slightly non-uniform (maximum corrosion depth 90-120 µm after 480 days) as in the case of the unwelded specimens. Severe local corrosion attacks in the welds or in the HAZ, as were determined on the only-welded specimens, were not observed on the thermal treated welded specimens.

In general it can be stated that, in contrast to the only-welded specimens, the thermal treated welded specimens show a sufficient resistance to local corrosion in the brine, and that their corrosion behaviour is similar to that of the parent material. As in the

case of the only-welded specimens, there are not noticeable differences in the corrosion behaviour of the thermal treated EB- and TIG-welded specimens.

Results in the NaCl-rich brine

Figure 3 shows the time-dependence of the general corrosion of the unwelded and only-welded steel specimens in the NaCl-rich brine at 150°C. As in the $MgCl_2$-rich "Q-brine", the thickness reduction of the specimens increases linearly with the exposure time in the brine. The linear corrosion rates of the unwelded and only-welded spacimens, calculated from the slope of the curves are compiled in Table 3. As in the $MgCl_2$-rich Q-brine, the corrosion rates of the welded specimens (18.6 µm/a – 19.1 µm/a) are very close to the value of the unwelded specimens (15.3 µm/a). The metallographic examinations of corroded specimens show that corrosion of the welded specimens is uniform, as in the case of the unwelded specimens. In general it can be stated that the corrosion behaviour of the EB- and TIG-welded steel specimens is very similar to that of the unwelded specimens.

The corrosion results obtained for the thermal treated welded steel specimens in NaCl-rich brine at 150°C are given in Figure 4 and Table 3. For comparison, the results obtained on unwelded and only-welded specimens are also given. The general corrosion of all specimens increases linearly with the exposure time during the whole test duration (Figure 4). The linear corrosion rates of the heat treated welded steel specimens of 22.6 µm/a – 25.9 µm/a (Table 4) are somewhat higher than the values of the unwelded and only-welded specimens (15.1 µm/a – 19.1 µm/a) as in the Q-brine. However, this increase in the values is not significant. The surface profiles and the metallographic examinations of the heat treated welded specimens do not show any signs of pitting corrosion.

In general it can be stated that considering an NaCl-rich brine as corrosion medium in a rock salt-repository, a heat treatment of the welds of steel containers is not necessary because it does not improve its corrosion behaviour.

The comparison of the corrosion rates of the steel in Q-brine and NaCl-rich brine (Tables 2 and 4) shows that the values in the $MgCl_2$-rich "Q-brine" are significatly higher than in the NaCl-rich brine. The higher corrosivity of the $MgCl_2$-rich brine is attributed to its higher HCl concentration. This could be explained by the higher Cl^- concentration and the hydrolysis of Mg^{2+}. The acceleration of the steel corrosion in brines containing high amounts of $MgCl_2$ is in line with the results reported by Westerman et al.[7].

2.1.2 Contact corrosion between Ti99.8-Pd and carbon steel in NaCl-rich brine (WP1.2) (FZK.INE)

A potential packaging design for vitrified HLW and spent fuel is the use of a double-wall container (overpack) surrounding the canisters. This consists of an inner thick-walled carbon steel container as mechanical support against the rock pressure which is corrosion protected by a thin-walled container made of the alloy Ti99.8-Pd. By use of a such metal combination and penetration of the outer steel container (e.g. by pitting corrosion) with resulting intrution of brine in the space between the containers, a contact corrosion can be established between the container materials. In this case, an increase in the corrosion rate of the less noble carbon steel and a decrease in the corrosion rate

of the more noble Ti99.8-Pd is expected. However, due to the formation of aggressive Fe^{3+} from the corrosion of the steel, a pitting corrosion of Ti99.8-Pd could occur. Under this aspect is investigated in this study whether under realistic disposal conditions (salt brines, high temperature) a contact corrosion occurs on the metal pair Ti99.8-Pd and TStE355 carbon steel (0.17 wt.% C).

Contact assemblies were formed by bolting one flat coupon of Ti99.8-Pd (40mm x 20mm x 4mm) with one flat coupon of carbon steel (40mm x 20mm x 4mm). The two coupons were provided with bores in both ends and were fastened with titanium-screws. The bores were isolated by PTFE. With this specimens type, the metals were joined very tight. The experiments were performed in autoclaves and the specimens were totally immersed in a NaCl-rich brine (25.9 wt.% NaCl, pH (25°C) = 6.5). The test temperature was 150°C and the maximum test duration about 18 months. Experiments were performed both with and without gamma radiation of 10 Gy/h. This dose rate corresponds to the value on the surface of the thick-walled container discussed.

Results

The thickness reduction (general corrosion) of the coupled specimens of Ti99.8-Pd and TStE355 carbon steel specimens in NaCl-rich brine at 150°C with and without gamma radiation is plotted in Figures 5 and 6. In both cases with and without gamma radiation the thickness reduction of the passive corroded alloy Ti99.8-Pd is negligible low (0.1 µm at the maximum).

The thickness reduction of the carbon steel in the brine with and without gamma radiation increases linearly with the exposure time (Figure 5 and 6). The calculated linear corrosion rates of the coupled specimens of Ti99.8-Pd and carbon steel in the NaCl-rich brine (T = 150°C) are given in Table 5. For comparison the values of uncoupled (single) specimens of these materials determined in previous investigations [5,6] are also given. For Ti99.8-Pd, the corrosion rates of the coupled specimens are negligible low (0.07 µm/a – 0.1 µm/a) and very close to the values of the uncoupled specimens (0.02 µm/a – 0.05 µm/a). In the case of the carbon steel the corrosion rates of the coupled specimens in NaCl-rich brine without radiation (14.2 µm/a) correspond very well to the values of the uncoupled specimens (15.3 µm/a). In the presence of a gamma radiation field of 10 Gy/h, the corrosion rate of the contact steel specimens in the brine is clearly lower (5.4 µm/a) than without irradiation. The lower corrosion rate under irradiation could be explained by the formation of a very dense protective oxide layer (Fe_3O_4) on the steel specimens in the contact area between steel and Ti99.8-Pd.

The metallographic examinations of coupled Ti99.8-Pd specimens do not show any signs of corrosion neither in the contact area to steel nor in the free specimen area. For the steel specimens, a slight non-uniform corrosion (20 – 30 µm after one year) was observed in the contact area to Ti99.8-Pd and in the free area of the specimens. In general, it can be stated that in the contact area no preferential corrosion attack was observed, compared to the free specimen area.

The results obtained indicate that the coupling of Ti99.8-Pd and TStE355 carbon steel does not accelerate the corrosion rate of the individual materials in NaCl-rich brine. This means that in this brine no serious contact corrosion between Ti99.8-Pd and TStE355 carbon steel is expected.

2.1.3 Electrochemical studies on Copper, Nickel and Copper-Nickel alloys (GNF,IUT)

Investigations on Cu in salt brines (WP1.5)

The electrochemical corrosion behaviour of copper (99.9 % Cu) was investigated in three disposal-relevant salt brines at 25°C. The salt brines used were: saturated NaCl-brine, $MgCl_2$-rich Q-brine (26.8 wt.% $MgCl_2$) and NaCl-rich brine (25.9 wt.% NaCl). In all brines potentiodynamic measurements were carried out. Moreover, potentiostatic measurements were performed in saturated NaCl-brine and $MgCl_2$-rich Q-brine and the rest potentials in these brines were determined. All the experiments were conducted under aerobic conditions.

From the results obtained so far under aerobic conditions at 25 °C, the following statements can be made. In the potential range between –1300 mV and –100 mV (SHE), Cu is in the brines in the passiv state. At a potential rate of 20 mV/s a valence change has been observed, which is attributed to the transition Cu (0) → Cu (I). At 1 mV/s this peak disappears in the voltammogram, a phenomenon to be understood by the assumption that Cu (I) is oxidized to the bivalent state by the oxygen still being present. Experiments carried out under anaerobic conditions will give a final answer.

In the Q-brine the passive range is shorter (from –1300 mV up to –200 mV), but the slope of the relevant current-potential-curve is smaller compared to those obtained in the other brines. No corrosion of Cu was observed in the passive range. In the active range (transpassive range), however, significantly higher corrosion rates were observed which should be due to the oxygen content transferring the Cu (I) to Cu (II) by forming chlorocomplexes. Work is in progress to quantify the corrosion rates. The rest potential of -100 mV (SHE) is in the transition area between active and passive range.

Potentiodynamic measurements on Ni in brines

Potentiodynamic measurements were performed on Ni in the $MgCl_2$-rich Q-brine and in the NaCl-rich brine in the temperature range between 25°C and 80°C.

The cyclovoltammograms show that Ni has in Q-brine and also in NaCl-rich brine a passive range from -700 mV to +100 mV, all potentials being referred to SHE (Figure 7). These results are in accordance with Vetter's data [8,9] obtained from measurements in diluted H_2SO_4, under the assumption that an amorphous NiO layer has been formed.

The relevant current densities are higher in the brines in the presence of argon than in those in the presence of oxygen or air (Figure 8). This results from the fact, that the current density "i" represents the sum of the positive and negative partial current densities ,the latter being higher in presence of oxygen due to its being reduced to OH^- or H_2O on a larger scale. Stirring increases the current density due to prohibiting areas of depletion near the electrode. In the transpassive range the corrosion rate is doubled by 300 rotations per minute and it is sixfold by 600 rotations per minute (Figure 9).

The influence of temperature in the range between 25°C and 80°C on the relevant current densities (Figure 10) is demonstrated by the fact, that the current densities increase at higher temperature. Moreover, a passive range even exists at 80 °C, although it is shortened at this comparatively high temperature. At higher temperatures the current densities are higher in aerobic atmosphere than under Argon, which proves that not the partial carthodic current density but the partial anodic current density becomes dominant. Although the influence of temperature on the passive range cannot be denied it must be emphasized that the passive range does not change under aerobic or anaerobic conditions, and it is not affected by stirring (Figure 10).

Potentiodynamic measurements on Cu-Ni alloys in Q-brine and NaCl-rich brine

The comparison of the Figures 11 and 12 demonstrates the dominant behaviour of Cu in the Cu/Ni = 70/30 alloy at 25°C. Without stirring the transport limited current density is reached at +500 mV, the sweep proving that Cu corrodes to the monovalent state, to be oxidized to Cu^{2+} in aqueous solution. The reduction from Cu^{2+} to Cu^{+} can definitely be seen from the cathodic sweep. The still existing passive range can be compared with that of Ni, although it is shifted a little bit more to the negative range and is definitely shorter, especially in Q-brine. In order to get a deeper insight, selective corrosion must be studied. Also in this case corrosion increases by temperature, although the characteristics of the voltammograms are not changed (Figure 13). The cyclovoltammograms of the Cu-Ni 90-10 alloys are very similar. In general it can be stated that copper hinders the formation of an oxide protection layer.

Potentiostatic measurements on Ni and Cu-Ni alloys in Q-brine and NaCl-rich brine at rest potential and 25°C

The rest potentials of the various materials do not differ significantly from each other in Q-brine and NaCl-rich brine (Table 6). They are in the range between -50 mV and -130 mV. They all are in the passive range. For Ni the rest potential in Q-brine is half of the value obtained in NaCl-rich brine. This effect cannot be referred to $NiCl_3^-$ and $NiCl_4^{2-}$ complex formation, shifting the potential at equilibrium to the negative range, because the chloride concentration in both of the electrolytic systems is nearly the same. But since the corrosion rate of Ni in NaCl-rich brine is doubled compared with that in Q-brine, the more negative rest potental should be due to the higher partial anodic current density in NaCl-rich brine, which might result from the minor stability of the NiO layer in this case. This fact can only be studied by applying impedance measurements to these investigations.

For the alloy Cu-Ni 70-30 in Q-brine the results are reciprocal to those aforementioned. The rest potential in the brine is -130 mV. In this case preferred selective corrosion of Ni occurs. The rest potentials of Cu-Ni 90-10 are identical in Q-brine and NaCl-rich brine. The relevant rest potentials were reached after approximately 20 hours. Only for Ni in NaCl-rich brine this time was extended up to 80 hours. All the corrosion rates are smaller than 17 µm/a, the only exception being that of Cu-Ni 90-10 in Q-brine with a corrosion rate of 30 µm/a, showing the weakening of the oxide NiO layer by the high Cu content. Further experiments have to be carried out to study the selective corrosion.

Potentiostatic measurements on Ni in Q-brine at various potentials and 25°C

The results obtained from the potentiostatic studies on Ni in Q-brine at 25°C under aerobic and anaerobic conditions are compiled in Table 7. In general it can be outlined, that within the passive range, which is relevant for the disposal conditions discussed, the corrosion rate is only several µm per year. In the transpassive range, the corrosion rate increases significantly especially at higher potentials (> 250 mV), becoming outstanding at +600 mV, a potential at which the whole electrode was destroyed by corrosion only leaving a Ni-ring behind. Table 7 shows that in the presence of oxygen, the corrosion rate increases up to 25 % with respect to that under anaerobic conditions. This result confirms the characteristics of the voltammograms which have been already discussed.

2.2 Corrosion studies in granitic-bentonite environment (WP2) (ENRESA-INASMET)

The objective of this work is to evaluate the susceptibility of three candidate waste package container materials to stress corrosion cracking (SCC), pitting, and crevice corrosion in granitic-bentonite environments. The studied materials are the high corrosion resistant nickel base material Hastelloy C-22 and the intermediate corrosion resistant Cu-OF and Cu-Ni 70-30 (Cu30Ni). The effects of chloride ion concentration and temperature are investigated. Slow Strain Rate Tests (SSRT), electrochemical and crevice corrosion tests are performed in order to assess the corrosion behaviour of the materials.

Materials and corrosion environment

The three materials investigated were delivered in the hot-rolled and normalized condition as plates (13-15 mm thickness) and bars (30 mm diameter). The materials were characterized by means of mechanical tests, chemical analysis and metallography examinations. The chemical composition and the mechanical properties of the materials are given in Tables 8 and 9. The chemical compositions vary slight for different product forms. The metallographic examinations show an austenitic structure with twins for HC-22 alloy. Cu-OF and Cu30Ni present a recrystalized equiaxic structure with some twins.

Besides the parent metal, Electron Beam Welded (EBW) and Gas Tungsten Arc Welded (GTAW) specimens of the three candidate materials (Figure 14) were also investigated in this study. In order to characterize the weldments produced, metallographic specimens transversal to the welded joint have been studied. Figure 14 shows Vickers microhardness chains along the welded joints. In general, a slight increase of the hardness value in the welded joint was observed with respect to that obtained for the base (parent) material.

The chemical composition of the synthetic granitic-bentonite water is given in Table 10. The effect of chloride concentration was studied by adding chloride as NaCl to the original solution shown in Table 10. The final chloride concentration ranged between 6,500 and 50,000 ppm. Deaereated granitic water was used in the electrochemical and SSR tests.

2.2.1 Stress corrosion cracking studies (WP2.2)

Experimental setup

The susceptibility to SCC was studied by means of the Slow Strain Rate Technique (SSRT). Tests were conducted according to the requirements described in ISO 7539-7 [10] and ASTM G 129 [11]. The testing equipment consists of constant extension rate tensile testing machines of 50 KN capacity and selectable crosshead speed within the range of 0.1 to 10^{-6} mm/s. Round tensile specimens of 6 mm diameter and 30 mm gauge length were machined. In the case of welded joints, specimens were taken in the transverse sense. The specimens were tested in the deaerated granitic water and in argon, as inert reference medium, at 90ºC and strain rates ranging from 10^{-5} to $2x10^{-7}s^{-1}$. After each test, the elongation, reduction of area, maximum load, true stress at fracture and time to fracture were measured in order to assess the loss of ductility of the studied materials. This was complemented by metallographic and fractographic analysis of tested specimens in order to identify secondary cracks on the fracture surface and in the gage section of the tested specimen.

Results

A summary of the data obtained in the SSRT for Hastelloy C-22 is shown in Table 11. Few tests have already been concluded due to the large duration of the SSR tests. In those who have been finished, no loss of ductility was observed for HC-22 specimens when tested in the granite environment with respect to the results obtained in argon. No secondary cracks were noticed in the metallographic and fractographic analysis. Figure 15 shows a totally ductile fracture surface of a HC-22 alloy specimen tested with a strain rate of $2x10^{-7}$ s^{-1} in granitic water with a chloride content of 50,000 ppm.

2.2.2 Electrochemical corrosion studies (WP2.3)

Experimental setup

Potentiodynamic polarization was the electrochemical technique used in order to obtain information on the corrosion rate, pitting susceptibility and passivity of the studied alloys. Potentiodynamic tests were conducted according to ASTM G-59 standard [12] and ISO/CD 17475 Test Method [13] in a electrochemical glass cell which contained both the metal to be investigated and the environment in which the polarization scan was going to be performed. This cell had ports through which the working electrode (test specimen), the platinum counter and a salt bridge connected to a Saturated Calomel reference Electrode (SCE) were inserted (Figure 16). An external heater was used to maintain the desired temperature. During the test, N_2 was continuously bubbled into the solution through a fritted glass tube in order to create a deaerated solution. Test specimens measuring 15 mm in diameter and 2 mm thickness, with a 600 grit finish, were mounted in a Teflon holder, leaving an area of $1cm^2$. Tests were performed in the simulated granitic water containing 6,500, 15,000 and 50,000 ppm of chloride at two different temperatures, 25°C and 90ºC.

To control the potential and to measure the current a potentiostat was used. Prior to the start of each test the E_{corr} of the specimen was measured. The potential scan

started from a potential -200 mV below E_{corr} and was increased at a rate of 0.167 mV/s. Once the current density reached a value of 10 mA/cm^2, the direction of the potential scan was reversed at the same scan rate. Results were plotted as a polarization curve of potential (V) vs. current density (Amp/cm^2). From this curve the corrosion potential E_{corr}, the pitting potential E_{pit} and the general corrosion rate, can be obtained. The value of E_{pit} denoted the electrochemical potential at which the applied current rapidly increases indicating the possibility of pit initiation. The uniform corrosion rate was calculated according to specifications provided in ASTM G-102 [14].

Results

The corrosion data obtained from the polarization curves of the three materials in the granitic environment at 25°C and chloride contents of 6,500, 30,000 and 50,000 ppm are shown in Table 12. For the copper base materials it was observed that, in general, an increase of chloride concentration increases general corrosion. It should be noted that in the case of passivation of the material, pitting or some other type of localized corrosion, the calculation of the corrosion rate according to ASTM G-102 is not representative. The calculation of uniform corrosion rates from electrochemical tests is useful in the case of materials with general corrosion behaviour. Figure 17 shows the polarization curves obtained in the potentiodynamic tests for the Cu-OF.

Metallographic examinations of tested specimens show thin oxide films for copper alloys. In the case of Cu30Ni alloy, a slight dealloying corrosion was observed when tested with chloride contents of 30,000 and 50,000 ppm (Figure 18). For HC-22 alloy a very adherent passive oxide film was observed. No pitting corrosion was observed for the three alloys at any of the tested conditions.

2.2.3 Crevice corrosion studies (WP2.3)

Experimental setup

Crevice assemblies were formed by bolting together flat test specimens with crevice formers made of Teflon (Figure 19), according to ASTM specifications G-78 [15]. The resulting assemblies were immersed in autoclaves containing the granitic-bentonite solution, with different chloride contents ranging from 6,500 to 50,000 ppm. The tests were conducted at 90°C and lasted 1, 6 and 12 months. Welded and base materials were evaluated for crevice corrosion. The specimens were weighed before and after testing in order to determine the corrosion rates.

Results

No damage has been observed for Hastelloy C-22 alloy when tested for 6 months in granitic water with a chloride content of 50,000 ppm. The HC-22 specimens show after the testing the same look as before testing (Figure 20). The Cu30Ni specimens show non-uniform general corrosion, with 10 microns as maximum penetration depth, but no localized attack is observed. In the case of Cu-OF specimens, when tested for one month, a slight crevice corrosion was observed located outside, but immediately adjacent to the teflon gasket. Figure 21, shows a SEM micrograph of the attacked area.

2.3 Corrosion studies in clay environments (WP3) (SCK.CEN)

In previous studies [5], electrochemical experiments were performed to evaluate the susceptibility of preselected candidate container (overpack) materials to pitting corrosion in solutions simulating deep geological clay environments under aerobic conditions. This is representative for the period immediately after closure of the underground repository. The influence of the content of various anions (chloride, sulphate and thiosulphate) was investigated. Two different temperatures were considered: 16°C, being the temperature of the Boom clay host rock formation at 225 metres below ground level, and 90°C, being an intermediate temperature in the near field surrounding the containers.

The aim of the present study is to evaluate the influence of the oxygen content (work package 3.1), elevated temperatures (work package 3.2), and radiolytic products (work package 3.3) on the localized corrosion behaviour of preselected candidate container materials. The experiments of work package 3.1 are performed in glove boxes, which operate under a controlled inert atmosphere (Ar). The content of dissolved oxygen in the test solutions is always kept below 10 ppb. The experiments of work package 3.2 are performed in autoclaves at 140°C under aerobic conditions.

During the reporting time, the following progress has been made in the work packages 3.1 and 3.2:

- anaerobic experiments at 90°C: the complete test matrix is finished for carbon steel TStE 355, stainless steel UHB 904L, Ni-alloys Hastelloy C-4 and C-22, and Ti-alloy Ti/0.2 Pd (Ti99.8-Pd).

- anaerobic experiments at 16°C: the complete test matrix is finished for carbon steel TStE 355, stainless steel UHB 904L, Ni-alloys Hastelloy C-4 and C-22, and Ti-alloy Ti/0.2 Pd.

- aerobic experiments at 140°C: the complete test matrix is finished for the stainless steel UHB 904L.

2.3.1 Materials and experimental techniques

Materials

The susceptibility of seven candidate container materials to localized corrosion was evaluated. These are: carbon steel TStE 355, stainless steels AISI 316L, AISI 316Ti, and UHB 904L, nickel alloys Hastelloy C-4 and Hastelloy C-22, and titanium alloy Ti/0.2Pd (TiGr-7). The chemical composition of these materials is given in Table 13.

Electrochemical techniques and setup

The experimental approach via electrochemical testing is twofold:

- on the one hand, cyclic potentiodynamic polarization (CPP) measurements are performed to provide three characteristic potentials: (i) E_{NP}, the critical pit nucleation potential or breakdown potential (i.e. the potential above which new

pits nucleate and grow), (ii) E_{PP}, the protection potential or repassivation potential (*i.e.* the potential above which existing pits can grow, but new pits cannot nucleate; beneath this potential, pits do neither grow nor nucleate), and (iii) OCP, open circuit potential (*i.e.* the potential that the metal assumes in the studied electrolyte under open circuit conditions). The protection potential is derived in two alternative ways: (i) E_{PP1}, the potential where the reverse scan intersects the forward scan or (ii) E_{PP2}, the potential, on the reverse scan, where the current density becomes zero, *i.e.* where the anodic current is equal to the cathodic current. The CPP technique was chosen because it provides a reasonable, rapid method for predicting the tendency of an alloy to suffer localized corrosion in the form of pitting.

- on the other hand, experiments were performed to monitor the free corrosion potential, E_{CORR}, as a function of time, in media representative for the underground repository conditions, because the OCP-values derived from the CPP curves do not represent the actual value encountered in the underground environment. The E_{CORR} namely depends on the environmental conditions (*e.g.* oxygen content – since the test solutions are purged with pure nitrogen, to remove the oxygen, the values of E_{CORR} may be too low in the case of aerobic measurements), the surface conditions (*e.g.* mass transport), *etc.* Also, an equilibrium is not obtained within the limited time span of a CPP measurement. E_{CORR} has been known to vary with time. Dunn et al. [16] found an increase of ~430 mV in a 1000 mg/L Cl^- solution for alloy 825 over the course of 600 days. The displacement of E_{CORR} in the noble direction with time is thought to be related to passive film thickening and changing film composition [17].

A combination of these two techniques is essential in establishing the corrosion behaviour of the candidate container (overpack) materials. This is realized by comparing the 'actual' value of E_{CORR} relative to E_{NP} and E_{PP}, which are determined from the CPP-curves:

- $E_{CORR} \geq E_{NP}$: immediate pitting problems;
- $E_{CORR} << E_{NP}$: no pitting will occur;
- $E_{CORR} < E_{NP}$: if E_{CORR} is close to E_{NP}, pitting can occur if the separation between E_{CORR} and E_{NP} is reduced, *e.g.* by changing the oxidizing power of the solution, at MnS inclusions (*i.e.* a local site with a higher potential), *etc.*;
- $E_{CORR} << E_{NP}$ and $E_{CORR} > E_{PP}$: the overpack material could suffer long-term corrosion problems because localized attack, once initiated, will not be able to repassivate;
- $E_{CORR} << E_{PP}$: pits can neither grow nor nucleate;

The experimental setup to perform CPP-measurements consists of a potentiostat/galvanostat, a computer, and a three-electrode corrosion cell, *viz.* a working electrode (*i.e.* a sample of the investigated material), a counter electrode (Pt), and a reference electrode (Ag/AgCl). The glass corrosion cell used to perform the experiments under anaerobic conditions (in a glove box) has a double wall for more efficient and precise temperature control. The experiments at 140°C were performed in an autoclave. As reference electrode, an internal Ag/AgCl electrode, completely constructed from Teflon®, was developed in cooperation with the Reactor Materials Department of SCK•CEN. The electrode consists of a silver wire onto one

end of which a AgCl layer is deposited electrolytically. This wire is placed inside a heat-shrunk Teflon® tube which is filled with 0.1M KCl. A ceramic plug ($MgO-ZrO_2$) maintains contact between the sensing element of the reference electrode and the test solution. The Teflon® heat shrinkable tubing provides the pressure balance between the internal electrolyte solution and the test solution in the autoclave. A schematic representation of the internal Ag/AgCl reference electrode is shown in Figure 22.

2.3.2 Results

Monitoring the free corrosion potential, E_{CORR}

Figure 23 shows the evolution of the free corrosion potential, E_{CORR}, as a function of time for stainless steel AISI 316L in synthetic clay water solutions representative for various repository conditions. In synthetic oxidized clay water solutions (SOCW), containing 1000 mg/L Cl^- and 216 mg/L SO_4^{2-}, under aerobic conditions, a more or less constant value was reached of approximately +320 mV (vs. SHE) after about three days. When changing the environment from aerobic to anaerobic, the free corrosion potential dropped to about +120 mV (vs. SHE). In synthetic interstitial Boom clay water solutions (SICW), containing 27 mg/L Cl^- and 0.2 mg/L SO_4^{2-}, under anaerobic conditions, the free corrosion potential dropped even further to about –10 mV (vs. SHE). These values were found to be only slightly dependant on the alloy composition (within the range of stainless steels studied). Of course, the obtained values can still only be used in a first approach. For a more precise determination of the E_{CORR}, experiments monitoring the free corrosion potential over much longer periods of time should be performed. However, this is not a part of the scope of this project.

Potentiodynamic measurements under anaerobic conditions at 16°C

Ti/0.2Pd, Hastelloy C-4, Hastelloy C-22 and UHB 904L are resistant in all solutions (even at levels of 50,000 mg/L Cl^-). The stainless steels AISI 316L and AISI 316Ti showed signs of pitting only in solutions with a Cl^- concentration of 20,000 mg/L and higher. Figure 24 shows the characteristic pitting potentials (E_{NP}, E_{PP1}, and E_{PP2}) for these alloys in SICW containing 0.2 mg/L SO_4^{2-} and varying Cl^--concentration at 16°C. From Figure 24, it can clearly be seen that E_{NP} is much higher than the free corrosion potential, E_{CORR}, under all circumstances, indicating that these alloys will not suffer immediate pitting problems under these conditions. However E_{PP2} drops below E_{CORR}, indicating that these alloys could suffer from long-term corrosion problems under these conditions (because under these conditions, once localized attack has initiated it will not be able to repassivate). The corrosion susceptibility for both alloys is similar in solutions containing a chloride content up to 20,000 mg/L. However, in solutions containing 50,000 mg/L Cl^-, AISI 316Ti has a higher pitting resistance: E_{NP} is about 200 mV more noble than for AISI 316L.

Potentiodynamic measurements under anaerobic conditions at 90°C

Only Ti/0.2Pd remained unaffected in all solutions (up to 50,000 mg/L Cl^-). The carbon steel TStE 355 exhibited uniform attack in all tested solutions (from 100-50,000 mg/L Cl^-). The susceptibility to pitting of the stainless steel UHB 904L increased with increasing chloride content. But under all conditions, E_{NP} and E_{PP} were situated well above the free corrosion potential. Therefore it can be concluded that under anaerobic conditions UHB 904L will not suffer corrosion problems under repository conditions in clay. Figure 25 shows the characteristic pitting potentials (E_{NP}, E_{PP1}, and E_{PP2}) for UHB 904L in SICW containing 0.2 mg/L SO_4^{2-} and varying chloride content at 90°C. For the Ni-alloys, Hastelloy C-4 and C-22, the CPP-curves show the hysteresis typical for the onset of pitting corrosion. This can be seen in Figure 26 and Figure 27 for Hastelloy C-4 and Hastelloy C-2 respectively. However, analysis of the surface, by optical microscopy, after the experiment revealed only a tarnished (yellow-orange spots) surface without evidences of pitting attack. This is illustrated on Figures 28 and 29 for Hastelloy C-4 and Hastelloy C-22 respectively. In some occasions, Hastelloy C-22 showed slight signs of intergranular attack (IGA, as can be seen in Figure 30. Thus, the hysteresis is probably the result of an alteration of the passive layer. In Figures 26 and 27, a current peak around 400-500 mV (vs. SHE) can be observed. This peak can probably be contributed to either (i) the Cr (III) to Cr (VI) transformation or (ii) $Ni(OH)_2$ to Ni_3O_4 transformation.

Potentiodynamic measurements under aerobic conditions at 140°C

So far, only the stainless steel UHB 904L has been tested under these conditions. The experiments at 16°C and 90°C were conducted during the previous EC-Project (Contract FI4W-CT95-0002). Figure 31 shows the CPP-curves for stainless steel UHB 904L in SOCW containing 216 mg/L SO_4^{2-} and 1000 mg/L Cl^- at 16, 90, and 140°C. It was found that pitting is easier initiated with increasing temperature: E_{NP} and E_{PP} shift towards lower potentials (towards the active region) as the temperature is increased. At 16°C, the polarization curve exhibits *negative* hysteresis, *i.e.* the current density is smaller during the backward scan than during the forward scan. This indicates that (i) the protective properties of the passive film have improved and (ii) a damaged passive film repairs itself. Pitting corrosion is not expected to occur because hysteresis is negative. This was confirmed with optical microscopy. Increasing the temperature from 90 to 140°C, shifts the E_{NP} significantly to more active potentials from +782 mV (vs. SHE) to +511 mV (vs. SHE). Comparing these values to the free corosion potential, E_{CORR} (i.e. +320 mV vs. SHE), it can be concluded that UHB 904L is not expected to suffer from pitting immediate after emplacement of the container in the underground clay repository. However, under these conditions, UHB 904L could suffer from long-term corrosion problems because the protection potential drops well below E_{CORR} (for both temperatures).

3. CONCLUSIONS

From the results obtained in these studies, the following conclusions can be drawn:

- In NaCl-rich brine (T=150°C), the welded TStE 355 carbon steel is subject only to general corrosion as the unwelded steel. On the contrary, in $MgCl_2$-rich brine besides general corrosion severe pitting corrosion occurred on the welds. However, according to the experimental results, pitting corrosion can be avoided in $MgCl_2$-rich brine by stress relief thermal treatment of the welds.

- By coupling of the alloy Ti99.8-Pd with the TStE 355 steel, no contact corrosion occurs in NaCl-rich brine (T=150°C).

- Cu and Cu-Ni alloys (90-10 and 70-30) have between 25°C and 80°C in salt brines a large passive range and, therefore, the corrosion rates are low (8-30 µm/a).

- In granitic-bentonite water at 25°C, Hastelloy C-22, Cu and Cu-Ni 70-30 are resistant to pitting corrosion. Furthermore, no crevice corrosion and stress corrosion cracking were observed on Hastelloy C-22 (T=90°C). In the case of Cu, a slight crevice corrosion was occurred.

- In clay water (anaerobic conditions) at 16°C, the materials Ti99.8-Pd, Hastelloy C-4, Hastelloy C-22 and the stainless steel UHB 904L are resistant to pitting corrosion. The stainless steels AISI 316L and AISI 316Ti suffer from pitting corrosion at a Cl^- concentration higher than 20,000 mg/l. At the higher temperature of 90°C, only Ti99.8-Pd is resistant to general and pitting corrosion. The TStE355 carbon steel exhibits general corrosion and the susceptibility of UHB 904L to pitting corrosion increases with increasing Cl^- content. However, no serious corrosion problems are expected for the UHB 904L steel under realistic disposal conditions in clay. The alloys Hastelloy C-4 and Hastelloy C-22 suffer from pitting corrosion in solutions containing more than 20,000 mg/l. At 140°C (aerobic conditions), the susceptibility of the UHB 904L to pitting is higher than at 90°C.

4. REFERENCES

[1] G.P.Marsh, G.Pinard-Legry, E.Smailos et al., "HLW Container Corrosion and Design," Proc. of the Second European Community Conf. and Radioactive Waste Management and Disposal, Luxembourg, April 22-26, 1985, p.314, R.A. Simon (Ed.), Cambridge University Press, EUR 10163 (1986).

[2] E.Smailos, W.Schwarzkopf, R.Köster and K.H.Grünthaler,"Advanced Corrosion Studies on Selected Packaging Materials for Disposal of HLW Canisters in Rock Salt," Proc. of the Symposium on Radioactive Waste Management 1988, Tucson, Arizona, USA, February 28-March 3, 1988, Vol.2, pp. 985-994, Arizona Board of Regents (1988).

[3] E.Smailos, I.Azkarate, J.A.Gago, P.Van Iseghem, B.Kursten, T.McMenamin, "Corrosion Studies on Metallic HLW Container Materials," Proc. of the 4th European Conf. on Management and Disposal of Radioactive Waste, Luxembourg, 25-29 March 1996, pp. 209-223, T.McMenamin (Ed.), EUR 17543 (1997).

[4] E.Smailos, W.Schwarzkopf and R.Storch,"Corrosion Studies on Packaging Materials for High-Level Waste Disposal in a Rock-Salt Repository," Proc. of the 12th Scandinavian Corrosion Congress and Eurocorr '92, Espoo, Finland, June 1992, pp. 327-338 (1992).

[5] E. Smailos, A. Martínez-Esparza, B. Kursten, G. Marx, I. Azkarate,"Corrosion Evaluation of Metallic Materials for Long-Lived HLW/Spent Fuel Disposal Containers," EUR-Report 19112 (1999).

[6] E. Smailos, J.A. Gago, I. Azkarate, B. Fiehn,"Corrosion Studies on Selected Packaging Materials for Disposal of Heat-Generating Radiactive Wastes in Rock-Salt Formations," FZKA-Report 5587 (1995).

[7] R.E. Westerman, J.H. Haberman et al.,"Corrosion and Environmental Characterization of Iron-Base Nuclear Waste Package Structural Barrier Materials," PNL-Report No. 5426 (1986).

[8] H. Kaesche," Die Korrosion der Metalle", Springer Verlag, Berlin-Heidelberg-New York (1979).

[9] K.J. Vetter, K. Arnold, Elektrochemie 64 (1962) 240, 407.

[10] Corrosion of metals and alloys – Stress corrosion testing. Part 7: Slow strain rate testing". ISO 7539-7, International Standard ISO 1989-12-01.

[11] "Standard Practice for Slow Strain Rate Testing to Evaluate the Susceptibility of metallic Materials to Environmentally Assisted Cracking", Standard G129, Annual Book of ASTM Standards, Vol.03.01; West Conshohocken, PA, ASTM.

[12] "Standard Reference Test Method for Making Potentiostatic and Potentiodynamic Anodic Polarization Measurements". Standard G5, Annual Book of ASTM Standards, Vol.03.02; West Conshohocken, PA, ASTM.

[13] "Corrosion of metals and alloys – Electrochemical test methods – Guidelines for conducting potentiostatic and potentiodynamic polarization measurements". COMMITTEE DRAFT, ISO/CD 17475, International Standard ISO 2001.

[14] "Standard Practice for Calculation of Corrosion Rates and Related Information from Electrochemical Measurements". Standard G102, Annual Book of ASTM Standards, Vol.03.02; West Conshohocken, PA, ASTM.

[15] "Crevice Corrosion Testing of Iron-Base and Nickel- Base Stainless Alloys in Seawater and other Chloride-Containing Aqueous Environments". Standard G78, Annual Book of ASTM Standards, Vol.3.01; West Conshohocken, PA, ASTM.

[16] D.S. Dunn, G.A. Cragnolino, and N. Sridhar,"An Electrochemical Approach to Predict Long-Term Localized Corrosion of Corrosion-Resistant High-Level Waste Container Materials, " *Corrosion* **56** (1), pp. 90-104 (2000).

[17] J.-H. Wang, C.C. Su, and Z. Szklarska-Smialowska,"Effects of Cl^- Concentration and Temperature on Pitting of AISI 304 Stainless Steel," *Corrosion* **44** (10), pp. 732-737 (1988).

5. MANAGEMENT AND CO-ORDINATION ASPECTS

Co-ordination was carried out in accordance with the obligations specified in Article 2 of Annex II to the contract (see also session 4.3 of Annex I to the contract).

Project Co-ordination meetings (PCM) were held on:

- 1 March and 2 March 2001 in Berlin ("Kick off meeting"). The minutes of the meeting were submitted to the EC on 22 March 2001.

- 8 October and 9 October 2001 in San Sebastian.

In accordance with the contract, the Technology Implementation Plan, TIP, (Preliminary version, three months after project start) was submitted to the EC on March 2001.

6. DEPARTURES FROM THE WORK PLAN

The updated time schedule of the work plan is shown in Annex.

The activities related to the work packages WP1 (Corrosion studies in salt environments; FZK.INE and GNF.IUT) and WP2 (Corrosion studies in granitic environments; ENRESA/INASMET) have been performed according to the time schedule given in the Technical Annex to the contract.

In the corrosion studies related to clay environments (WP3) the technical content of tasks 3.1 (Influence of anaerobic conditions) and 3.2 (Influence of elevated temperature) was slightly modified. The test matrix for the experiments in synthetic bentonite clay water was expanded (compared to the test matrix as given in the Technical Annex to the contract) by variation of the thiosulphate concentration from 20 mg/L to 200 mg/L. A delay of about three months for task 3.1 was caused due to infrastructure problems at SCK.CEN. However, in order to avoid a delay of the whole project duration of 36 months, a part of the experiments under task 3.2 was already performed which were planned to start from month 11. The period for task 3.1 was extended for three months.

7. PLANNED ACTIVITIES FOR THE NEXT REPORTING PERIOD

Corrosion studies in salt environments (WP1)

- Continuation and completion of the experiments to the contact corrosion between carbon steel and Ti99.8-Pd in salt brines.
- Performance of long-term corrosion studies on Cu-base materials in salt brines.
- Electrochemical studies of the contact corrosion of Cu, Ni and Cu-Ni alloys with carbon steel.

Corrosion studies in granitic-bentonite environments (WP2)

- Slow strain rate tests (SRRT) on Hatelloy C-22, Cu-OF and Cu30Ni.
- Crevice corrosion tests at various Cl^- concentrations of the corrosion medium.
- Conclusion of the potentiodynamic polarization tests at 90°C.

Corrosion studies in clay environments (WP3)

- Completion of the anaerobic experiments at 16°C and 90°C.
- Continuation of the aerobic experiments at 140°C (solutions containing 20,000 and 50,000 mg/L Cl^-).

8. LIST OF DISTRIBUTED PAPERS

Title	Date	Addressee
TIP preliminary version	30 January 2001	EC, Partners
Agenda 1st PCM	30 January 2001	Partners, EC
Minutes 1st PCM	22 March 2001	Partners, EC
1st management report	23 May 2001	EC, Partners
Agenda 2nd PCM	3 August 2001	Partners, EC
Minutes 2nd PCM	6 November 2001	Partners, EC

TIP = Technology Implementation Plan
PCM = Project Coordination Meeting

Table 1: Influence of welding on corrosion of TStE355 steel in $MgCl_2$-rich brine (Q-brine) at 150°C and a gamma-dose rate of 10 Gy/h

Material condition	Max. test duration (d)	Linear corrosion rate (µm/a)	Max. local corrosion (µm)		
			Base mat.	HAZ	Weld
unwelded	550	72.6 ± 11	60	—	—
EB-welded	300	67.7 ± 41	90	1500	1200
TIG-welded	300	65.8 ± 40	180	1250	1350

HAZ= Heat Affected Zone

Table 2: Influence of welding and heat treatment on corrosion of TStE355 steel in $MgCl_2$-rich brine (Q-brine) at 150°C and a gamma-dose rate of 10 Gy/h

Material condition	Max. test duration (d)	Linear corrosion rate (µm/a)	Max. local corrosion (µm)		
			Base mat.	HAZ	Weld
unwelded	550	72.6 ± 11	60	—	—
EB-welded	300	67.7 ± 41	90	1500	1200
TIG-welded	300	65.8 ± 40	180	1250	1350
EB-welded and heat treated *	480	94.7 ± 31	80	90	100
TIG-welded and heat treated *	480	112 ± 49	100	120	100

*2h,600°C

Table 3: Influence of welding on corrosion of TStE355 steel in NaCl-rich brine at 150°C

Material condition	Max. test duration (d)	Linear corrosion rate (µm/a)
unwelded	585	15.3 ± 1.0
EB-welded	506	18.6 ± 0.7
TIG-welded	506	19.1 ± 1.0

Table 4: Influence of welding and heat treatment on corrosion of TStE355 steel in NaCl-rich brine at 150°C

Material condition	Max. test duration (d)	Linear corrosion rate (µm/a)
unwelded	585	15.3 ± 1.0
EB-welded	506	18.6 ± 0.7
TIG-welded	506	19.1 ± 1.1
EB-welded and heat treated *	463	25.9 ± 7.0
TIG-welded and heat treated *	463	22.6 ± 6.8

* 2h,600°C

Table 5: Comparison of the corrosion of coupled and uncoupled specimens of Ti99.8-Pd and TStE355 steel in NaCl-rich brine at 150°C

Material	Corrosion conditions	Corrosion rate (µm/a)	
		coupled specimens	uncoupled specimens
Ti99.8-Pd	NaCl-brine	0.07 ± 0.01	0.02 ± 0.01
	NaCl-brine/10 Gy/h	0.10 ± 0.05	0.05 ± 0.02
TStE355 steel	NaCl-brine	14.2 ± 1.6	15.3 ± 1.0
	NaCl-brine/10 Gy/h	5.4 ± 0.5	13.5 ± 1.8

Table 6: Corrosion results on Ni and Cu-Ni alloys from potentiostatic measurements in brines at rest potentials and 25°C under aerobic conditions

Material	Brine	Rest corrosion potential [SHE] (mV)	Δm [weight loss] (mg)	Time (h)	Corrosion rate (µm/a)
Ni	Q	-50 ± 5	0.10	230	8
Ni	NaCl-rich	-106 ± 8	<0.05	70	<14
Cu-Ni 70-30	Q	-130 ± 5	0.20	225	17
Cu-Ni 90-10	Q	-123 ± 4	0.15	96	30
Cu-Ni 90-10	NaCl-rich	-126 ± 4	<0.05	70	<14

Table 7: Corrosion results on Ni from potentiostatic measurements in Q-brine at various potentials and 25°C under aerobic and anaerobic conditions

Brine	Potential [SHE] (mV)	Time (h)	Δm [weight loss] (mg)	Corrosion rate (µm/a)
Q (air)	-546	8	<0.05	<123
Q (air)	-296	50	<0.05	<20
Q (air)	+4	48	<0.05	<20
Q (air)	+254	78	307	77×10^3
Q (air)	+254	10	91	179×10^3
Q (air)	+404	52	123	46×10^3
Q (air)	+604	52	137	52×10^3
Q (air)	+804	10	96	188×10^3
Q (Argon)	+604	48	730	302×10^3
Q (air)	+604	48	1001	414×10^3

Table 8: Materials investigated in granitic-bentonite water

Weight composition (%)	HC-22 (UNS N06022)		Cu-OF (UNS C10200)		Cu30Ni (UNS C71500)	
	Plate	Bar	Plate	Bar	Plate	Bar
Ni	*Base*	*Base*	<0.01	<0.01	30.2	30.0
Cr	21.8	21.6				
Mo	13.3	13.0				
W	3.0	3.0				
Fe	2.8	2.9	<0.01	<0.01	0.65	0.73
Cu	0.03	0.08	*Base*	*Base*	*Base*	*Base*
Co	0.38	0.95				
Al	0.22	0.19			<0.01	<0.01
V	0.16	0.14				
C	0.014	0.003			0.005	0.020
Mn	0.22	0.26	<0.01	<0.01	0.69	0.68
P	0.01	<0.01	<0.01	<0.01	<0.01	0.01
O			0.019	0.027	0.006	0.005

Table 9: Mechanical properties of the materials investigated in granitic-bentonite water. (L=Longitudinal ;T=Transversal)

Alloy		Yield Strength (MPa)	Maximum load (MPa)	Elongation (%)	Hardness (Vickers HV 10Kg)
Cu-OF	L	261	266	24	92
	T	268	283	25	
Cu30Ni	L	138	367	49	86
	T	121	362	49	
HC-22	L	370	755	76	181
	T	381	730	73	

Table 10: Composition of simulated granitic-bentonite water (pH (25°C) = 7.3)

Parameter	Composition (mg/l)
Cl^-	6550±250
NO_3^-	110±10
SO_4^{2-}	1500±30
HCO_3^-	27±5
SiO_2	8.3±0.5
Br^-	15±1
Ca^{2+}	135±10
K^+	20±1
Mg^{2+}	600±30
Na^+	3750±100

Table 11: SSRT data obtained for the alloy HC-22 tested at 90°C and a strain rate of $2x10^{-7}s^{-1}$

	HC-22 / $2x10^{-7}$ s^{-1}	
	Argon	Granitic water 50,000 ppm Cl^-
Reduction of Area (%)	78.5	76.7
Yield Strength (MPa)	338	330
Maximum Load (MPa)	741	729
True Stress at Fracture (MPa)	2002	1850
Time to rupture (h)	1580	1394
Secondary cracks	None	None
Failure mode	Ductile	Ductile

Table 12: Corrosion data from electrochemical polarization tests.

Material	Deaerated granitic water / 25°C				
	Cl^- (ppm)	E_{corr} (V_{SCE})	Corr. rate (µm/a)	$E_{Pitting}$ ($V_{vs\ SCE}$)	Surface appearance
Cu-OF	6,550	-0.28	11	-	General corrosion
	15,000	-0.34	14	-	"
	50,000	-0.32	86	-	"
Cu30Ni	6,550	-0.26	21	-	Bright / light scale
	15,000	-0.28	-	-	General corrosion / dealloying
	50,000	-0.35	65	-	General corrosion / dealloying
HC-22	6,550	-0.41	7	-	Bright / light scale
	15,000	0.37	3	-	"
	50,000	0.25	1	-	"

Table 13: Chemical composition of the candidate container materials investigated in clay environments (wt.%)

	Chemical composition (wt%)										
	Fe	Cr	Ni	Mo	Mn	Si	Ti	C	S	P	Others
Carbon steel											
TStE 355	bal	0.030	0.030	-	1.12	0.344	0.003	0.180	0.002	0.010	Nb 0.017; N_2: 0.005
Stainless steel											
AISI 316L	bal	16.90	11.00	2.08	1.54	0.54	-	0.017	0.001	0.032	
AISI 316Ti	bal	16.80	10.70	2.05	1.08	0.40	0.3	0.044	0.009	0.028	
UHB 904L	bal	19.70	25.00	4.47	1.48	0.19	-	0.019	0.001	0.019	Cu:1.51;N_2:0.080
Nickel alloys											
Hastelloy C4	0.98	15.75	bal.	15.85	0.04	0.02	<0.01	0.003	0.003	0.004	Co:0.01
Hastelloy C22	2.8	21.8	bal.	13.3	0.22	-	-	0.014	0.005	0.01	Co:0.38;W:3.0
Titanium alloy											
Ti/0.2Pd	0.04	-	-	-	-	-	bal	0.01	-	-	Pd:0.16;O_2:0.13; N_2<0.01;H_2:0.001

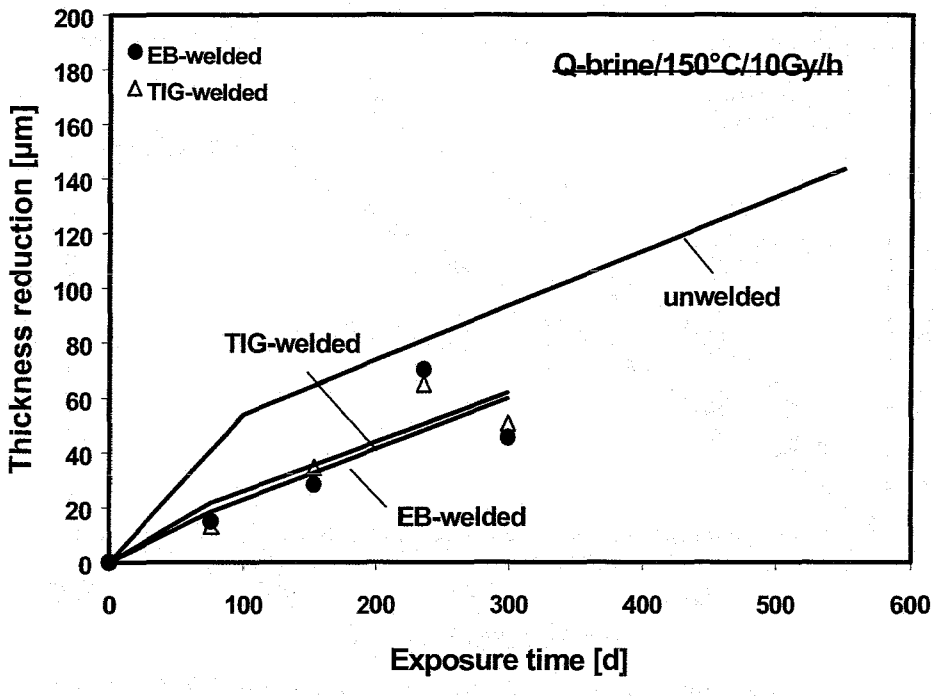

Figure 1: General corrosion of welded and unwelded TStE355 steel in $MgCl_2$-rich Q-brine at 150°C and 10 Gy/h

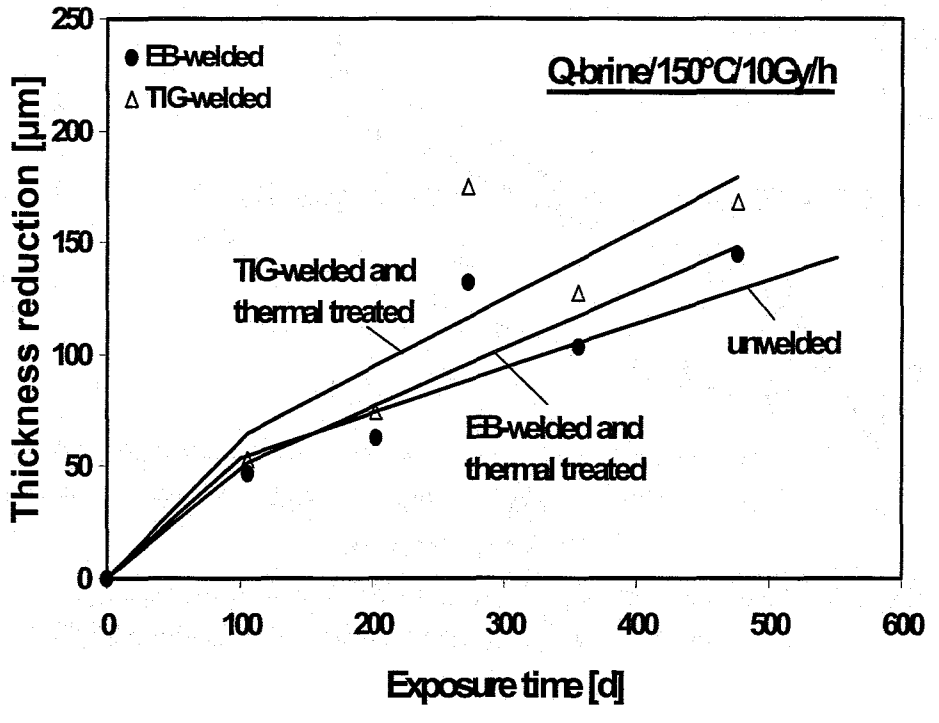

Fig. 2: General corrosion of unwelded and thermal treated welded TStE355 steel in MgCl-rich Q-brine at 150°C and 10 Gy/h

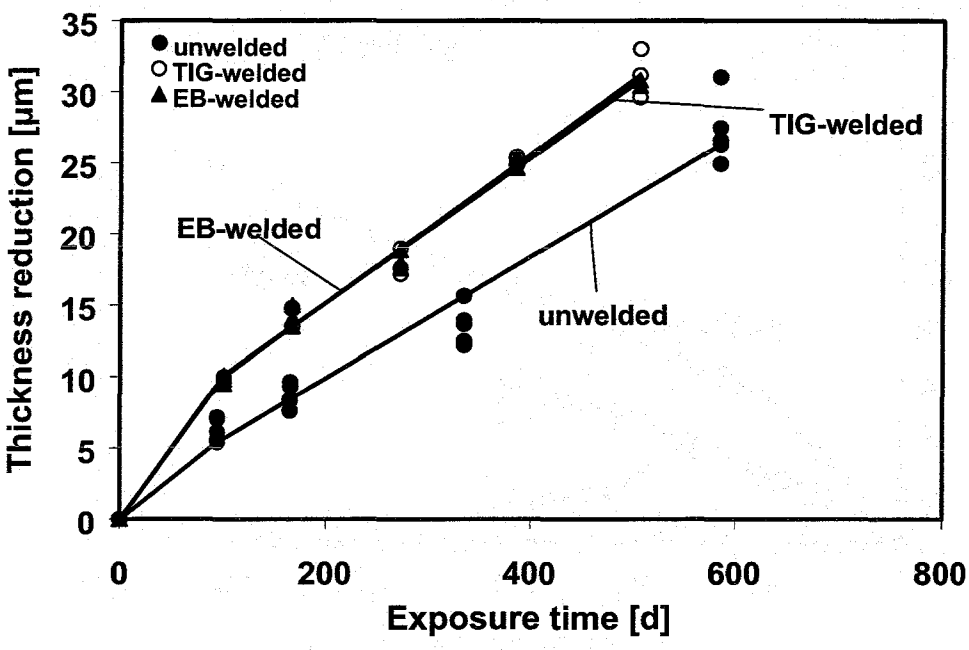

Figure 3: General corrosion of welded and unwelded TStE355 steel in NaCl-rich brine at 150°C

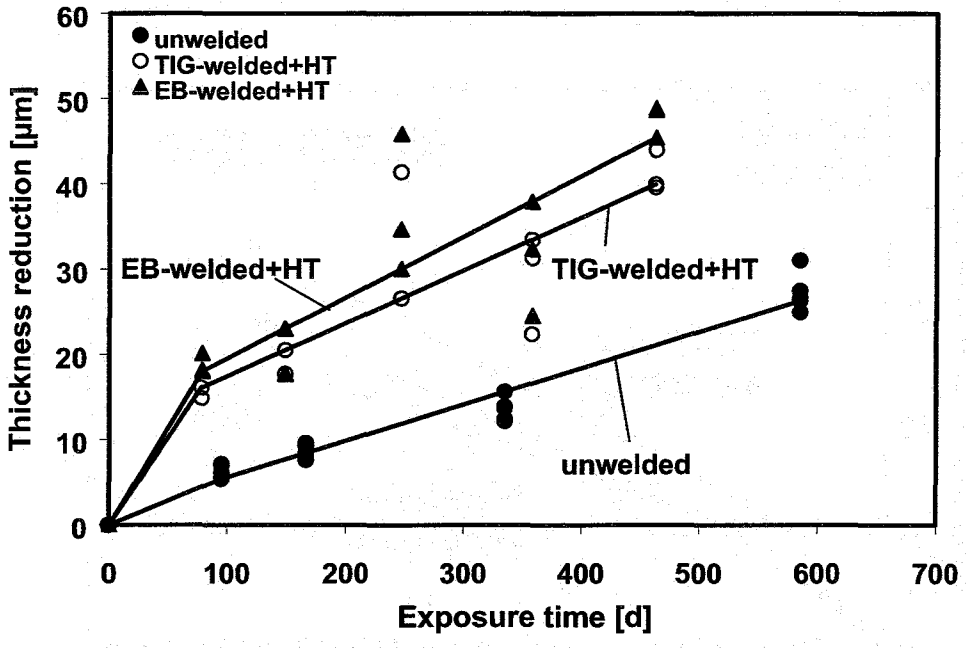

Figure 4: General corrosion of unwelded and thermal treated (HT) welded TStE355 steel in NaCl-rich brine at 150°C

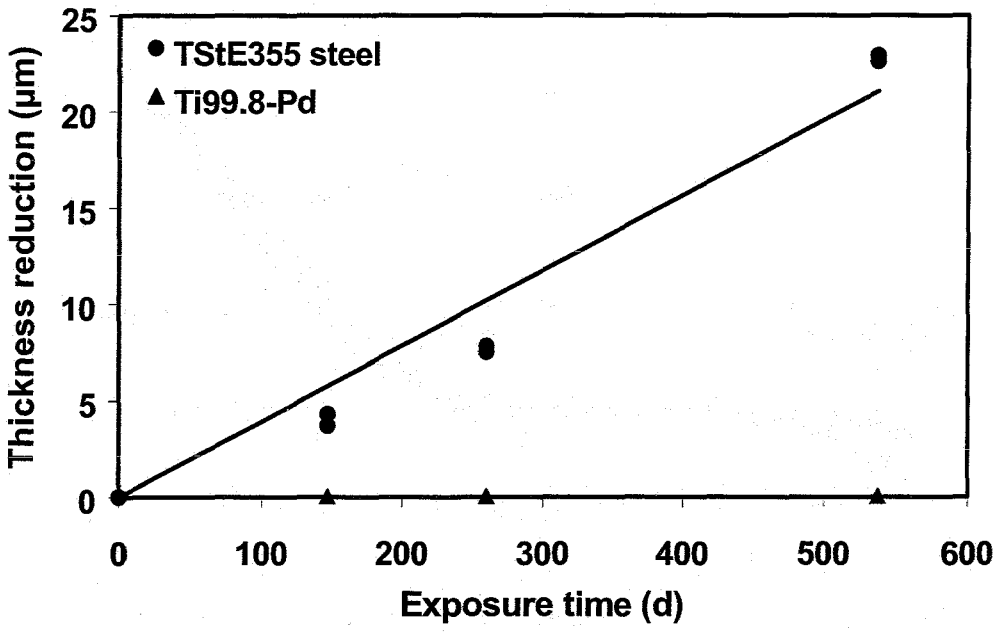

Figure 5: Contact corrosion of Ti99.8-Pd and TStE355 steel in NaCl-rich brine at 150°C

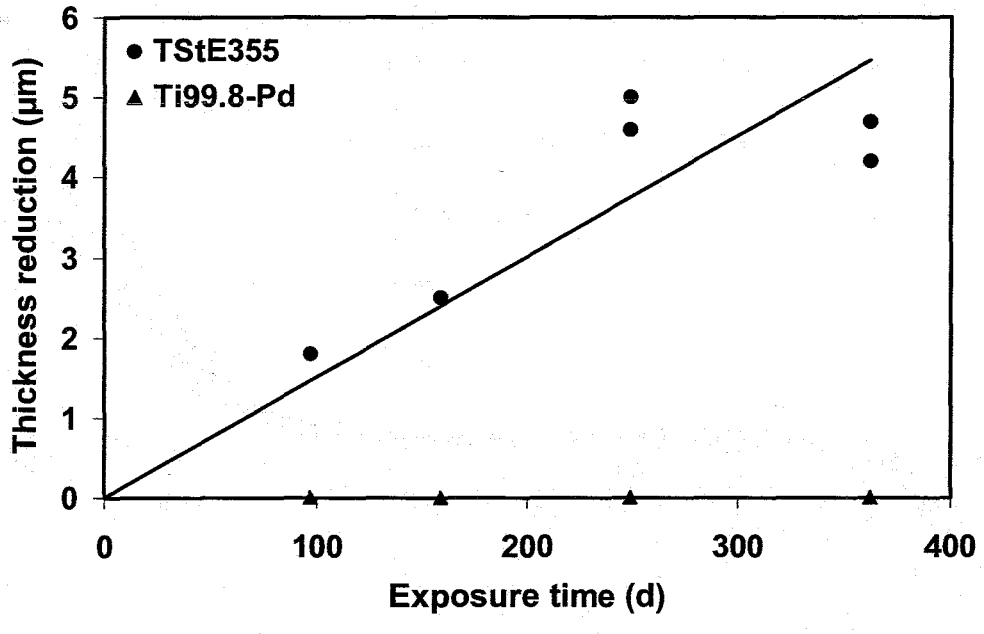

Figure 6: Contact corrosion of Ti99.8-Pd and TStE355 steel in NaCl-rich brine at 150°C and 10 Gy/h

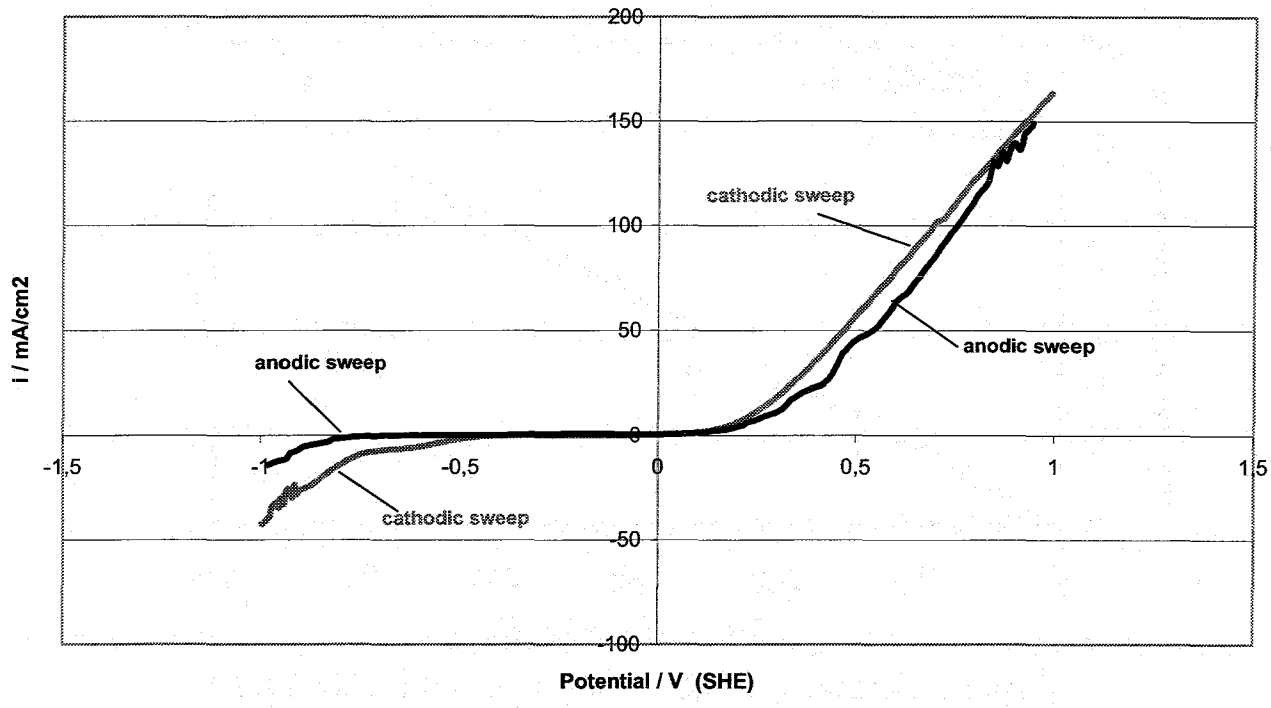

Figure 7: Cyclovoltammogram of Ni in Q-brine at 10 mV/s and 25 °C (aerobic conditions)

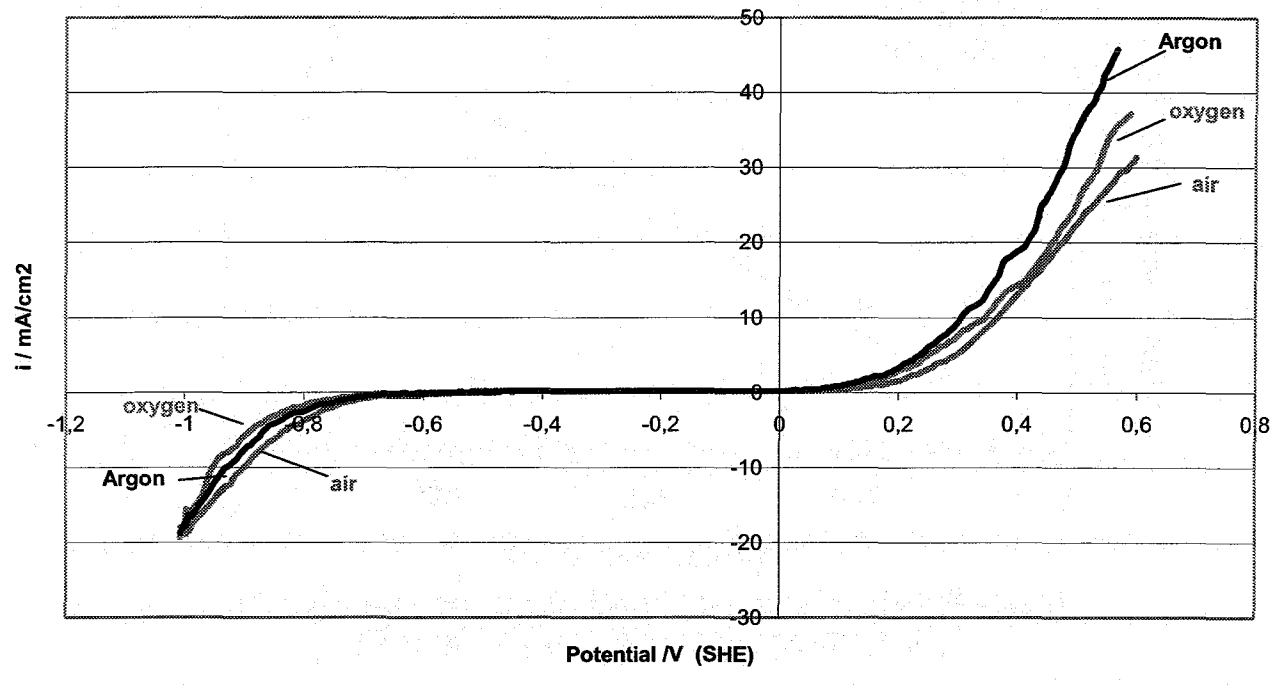

Figure 8: Cathodic Sweeps of Ni in Q-brine at 25 °C, 10 mV/s and a stirring rate of 300 rotations/min (U/min); influence of the kind of gas

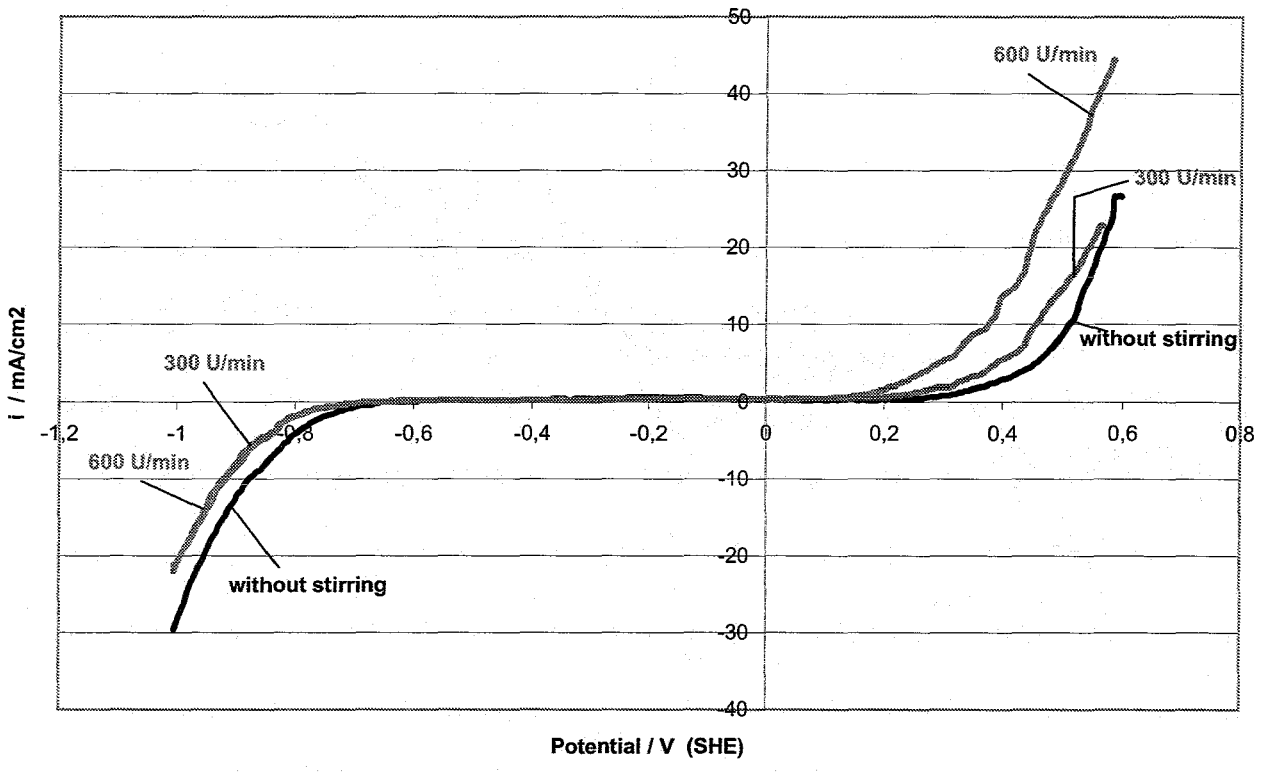

Figure 9: Anodic sweeps of Ni in Q-brine at 10 mV/s and 25°C (aerobic conditions); influence of stirring

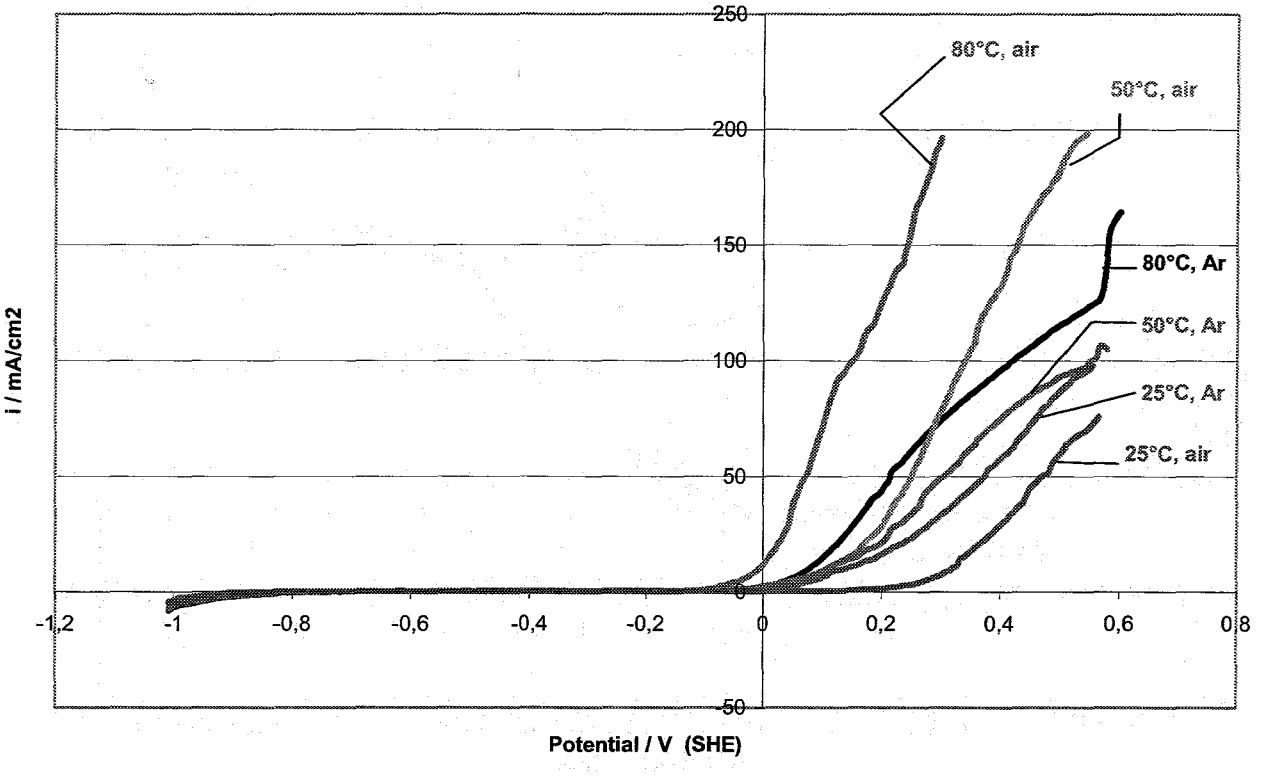

Figure 10: Anodic sweeps of Ni in NaCl-rich brine at 10 mV/s (aerobic conditions); influence of temperature

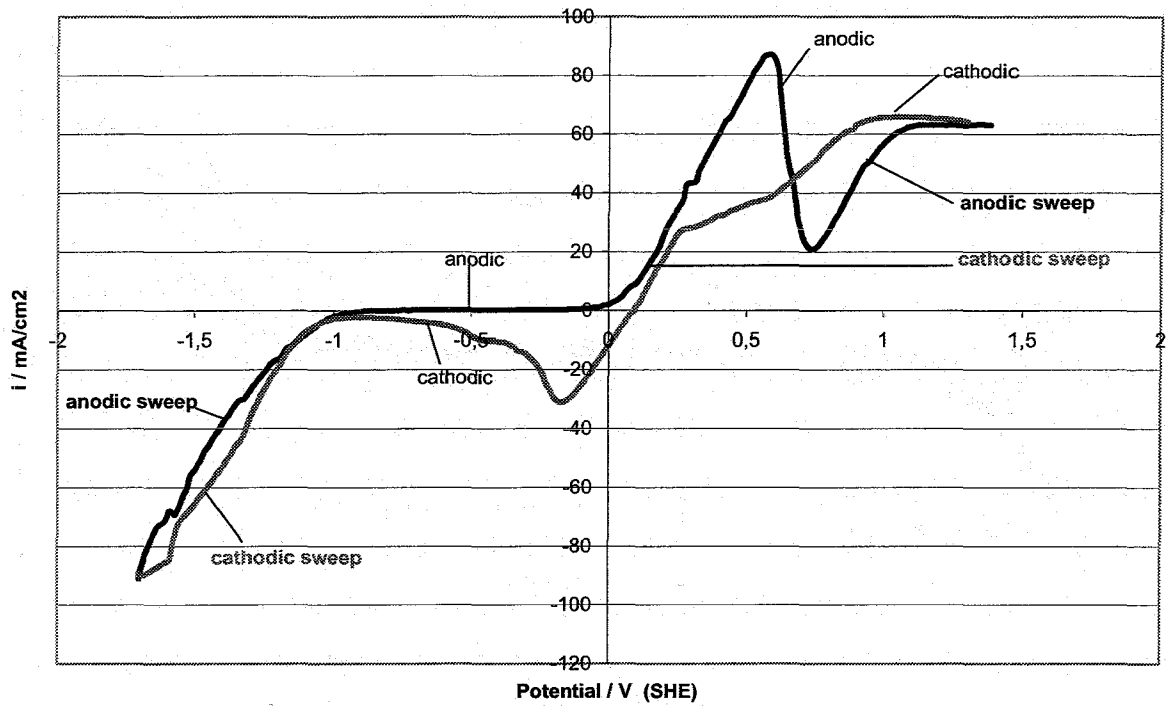

Figure 11: Cyclovoltammogram of Cu in Q-brine at 25°C and 10 mV/s (aerobic conditions)

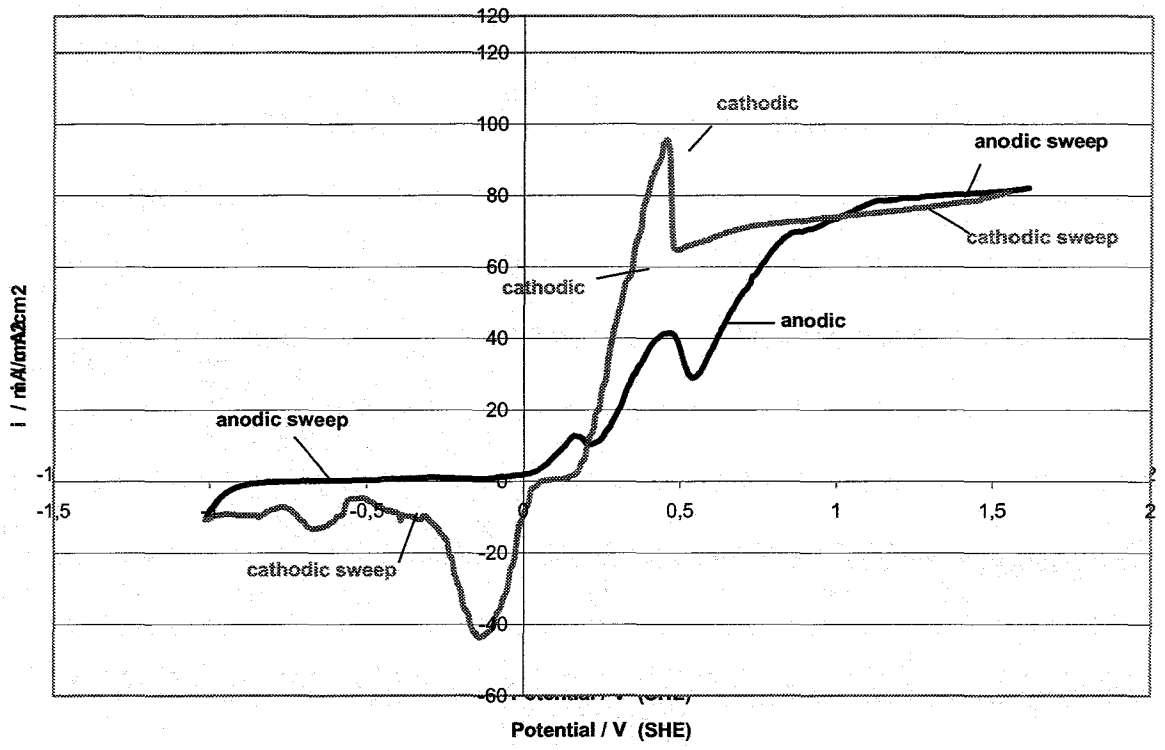

Figure 12: Cyclovoltammogram of Cu-Ni-alloys (Cu-Ni 70-30) in NaCl-rich brine at 10 mV/s and 25 °C(aerobic conditions); without stirring

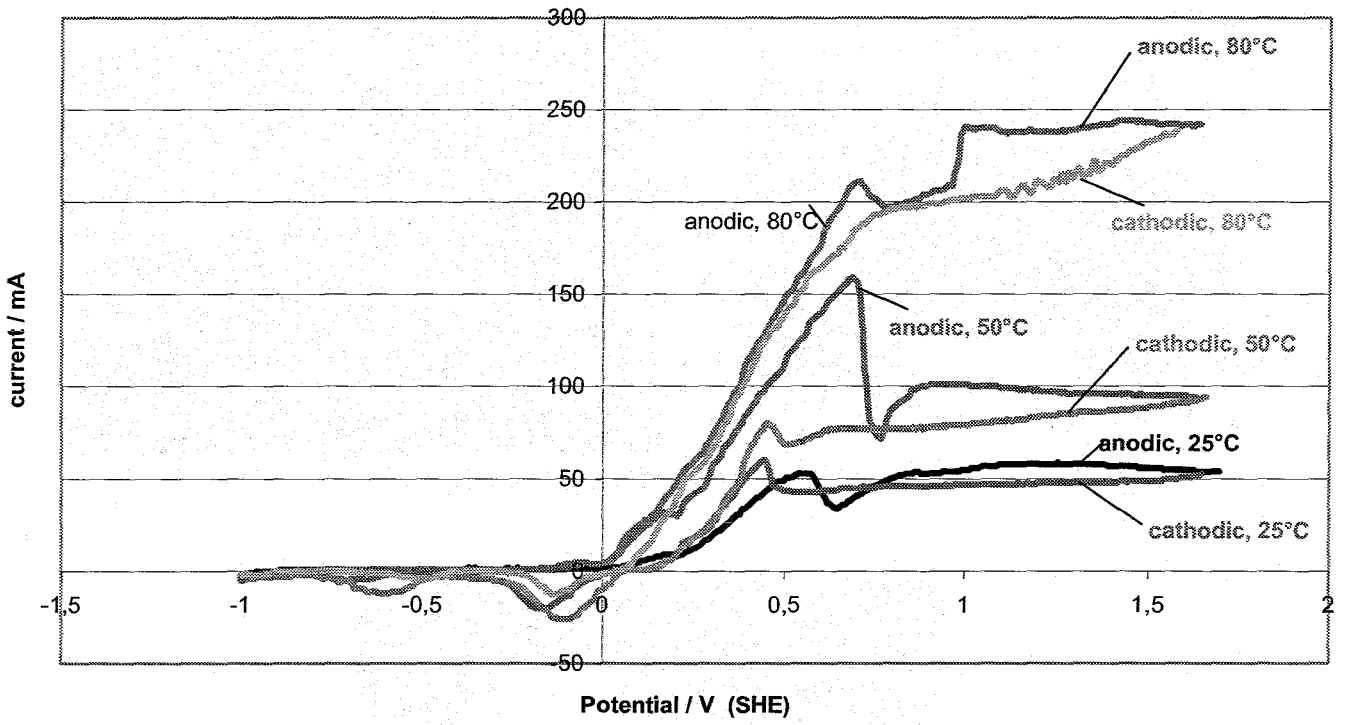

Figure 13: Cyclovoltammogramms of Cu-Ni-alloys (Cu-Ni 70-30) in NaCl-rich brine at 10 mV/s (aerobic conditions); influence of temperature

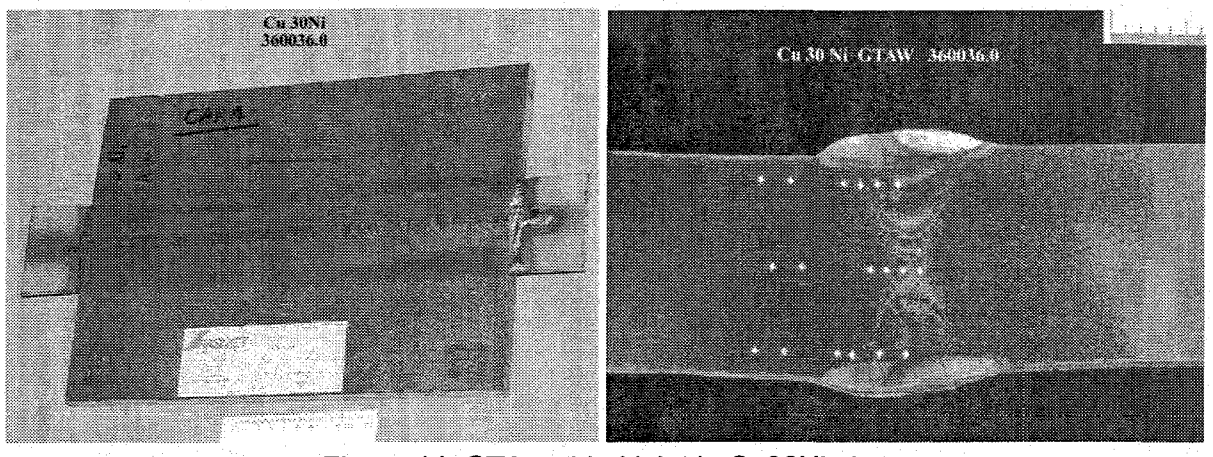

Figure 14. GTA welded joint in Cu30Ni plate.

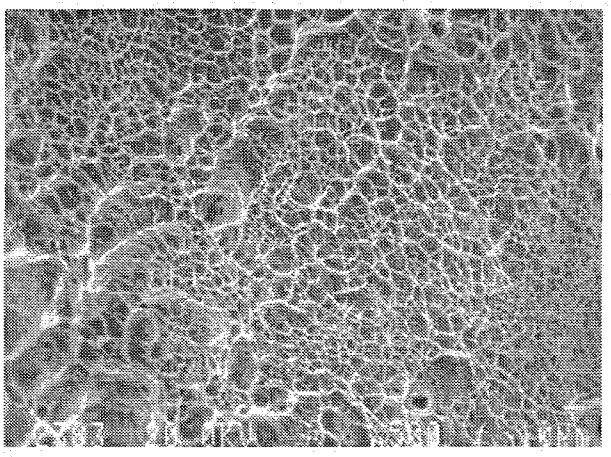

Figure 15. SEM micrograph of the fracture surface of a HC-22 alloy specimen tested at a strain rate of $2x10^{-7}$ s^{-1} in granitic-bentonite water with a chloride content of 50,000 ppm (x500).

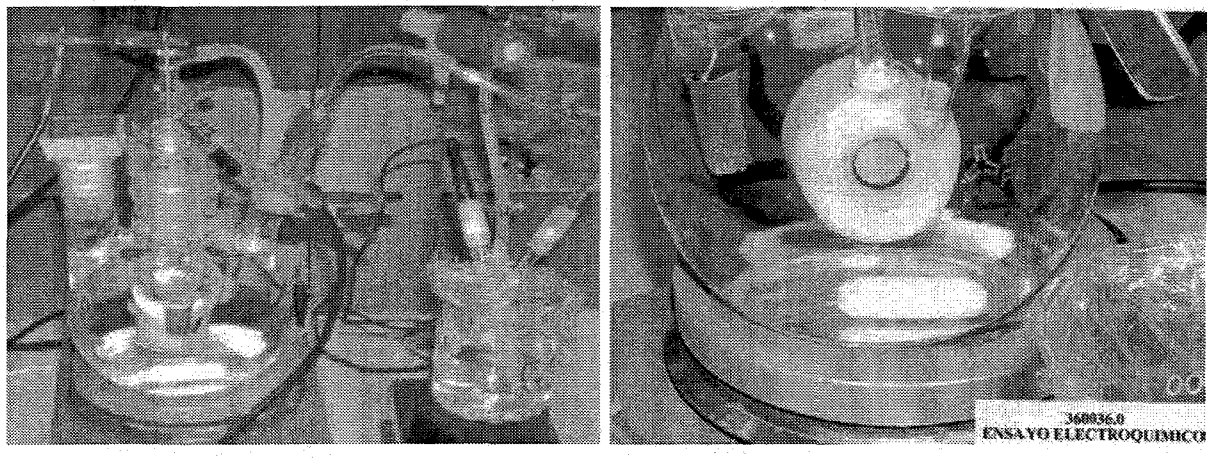

Figure 16. Electrochemical polarization cell for the experiments in granitic-bentonite water

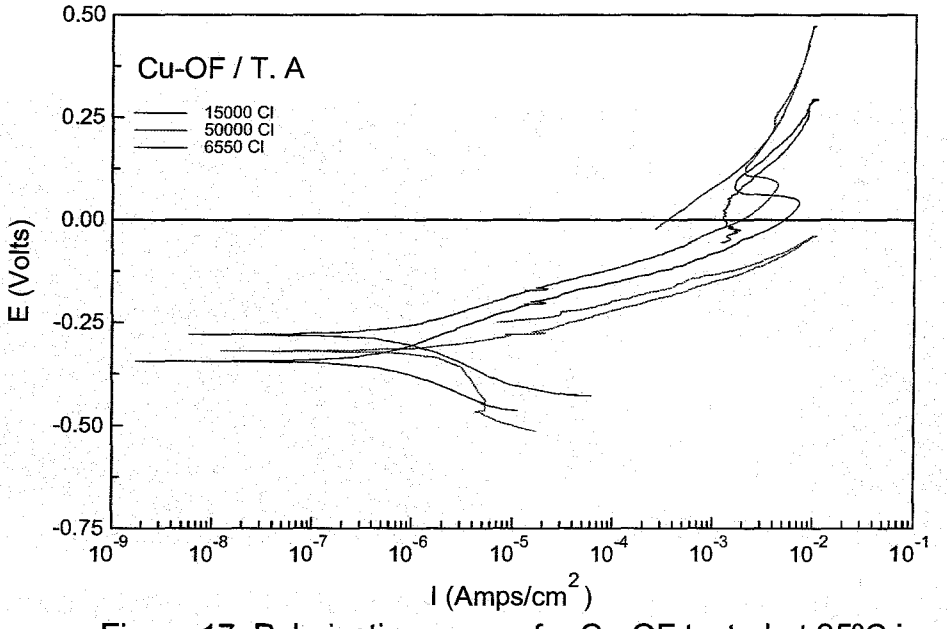

Figure 17. Polarization curves for Cu-OF tested at 25°C in granitic-bentonite water with various chloride contents.

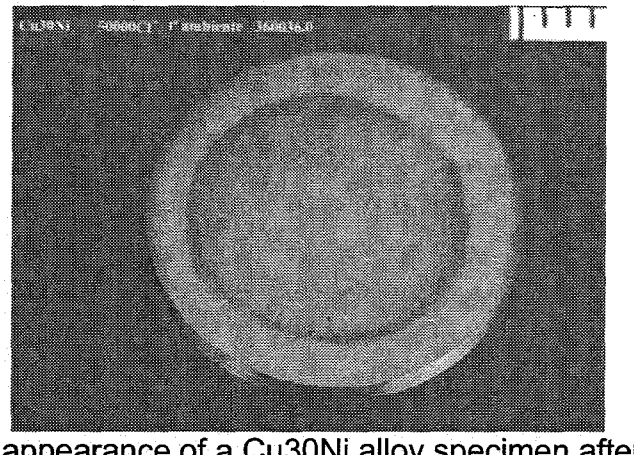

Figure 18. Surface appearance of a Cu30Ni alloy specimen after potentiodynamic polarization test.

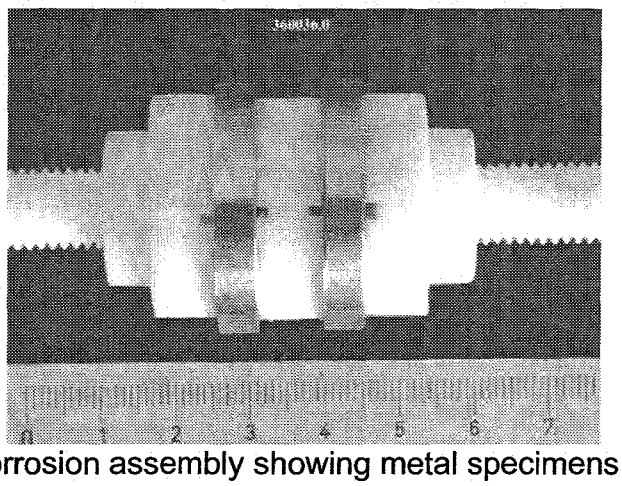

Figure 19. Crevice corrosion assembly showing metal specimens and Teflon gaskets.

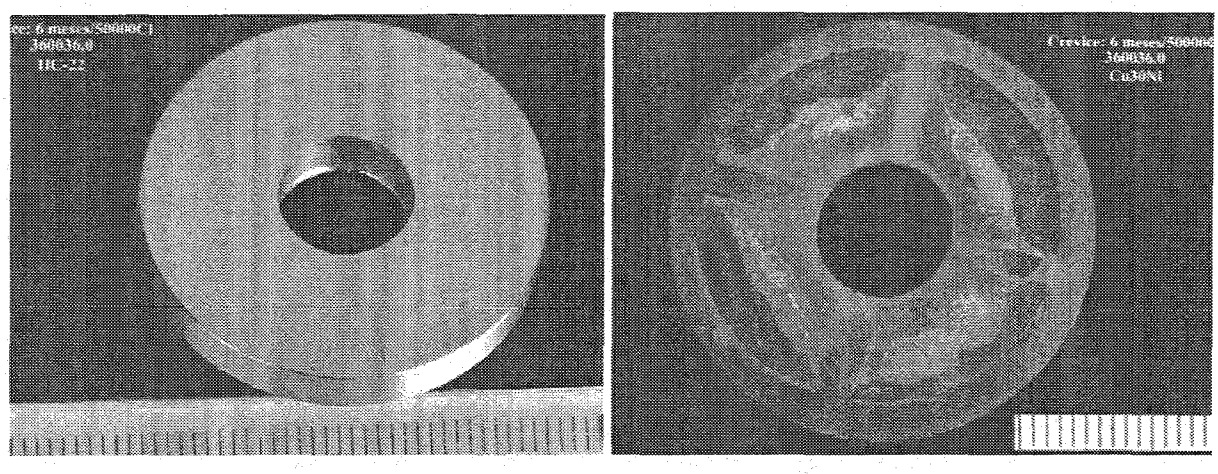

Figure 20. HC-22 and Cu30Ni crevice specimens after six months exposure in granitic water at 90°C and a chloride content of 50,000 ppm.

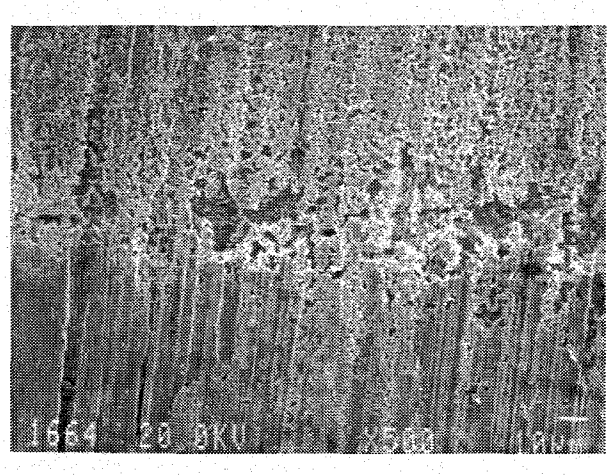

Figure 21. SEM micrograph showing slight crevice attack in Cu-OF specimen after one month in granitic water at 90°C and a Cl^--content of 15,000 ppm.

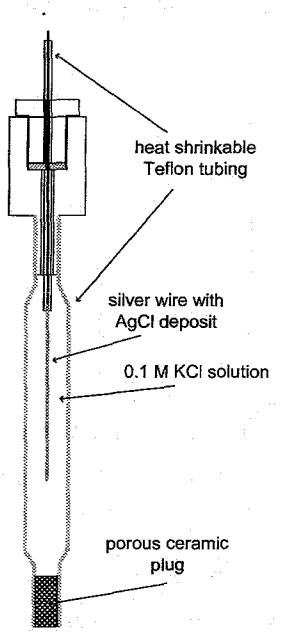

Figure 22: Schematic drawing of the internal Ag/AgCl reference electrode used to perform CPP-measurements at 140°C in an autoclave

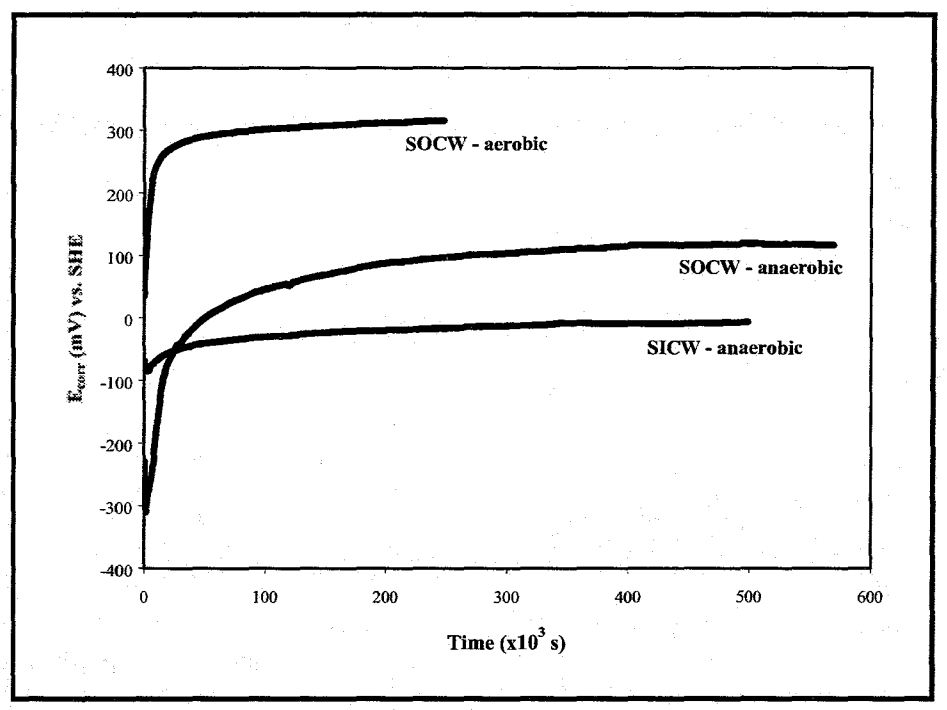

Figure 23: The evolution of the free corrosion potential (E_{CORR}) as a function of time for stainless steel AISI 316L in (i) synthetic oxidizing clay water (SOCW) under aerobic conditions (90°C), (ii) synthetic oxidizing clay water (SOCW) under anaerobic conditions (16°C), and (iii) synthetic interstitial clay water (SICW) under anaerobic conditions (16°C).

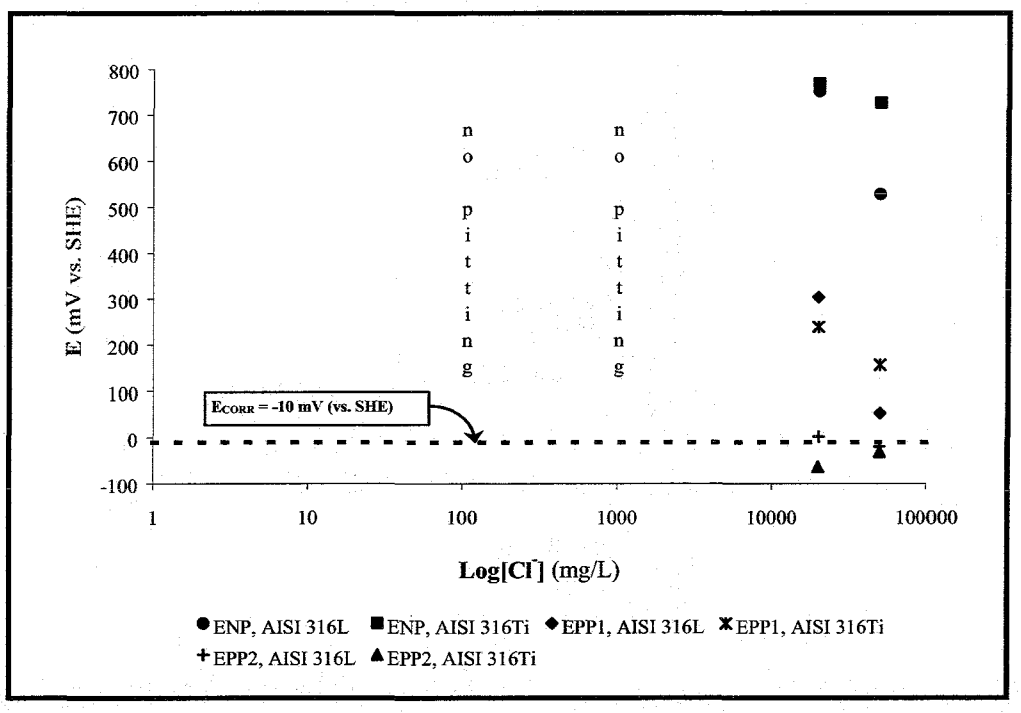

Figure 24: The characteristic pitting potentials (E_{NP}, E_{PP1}, and E_{PP2}) for stainless steel AISI 316L and AISI 316Ti in SICW containing 0.2 mg/L SO_4^{2-} and varying Cl^--concentrations at 16°C.

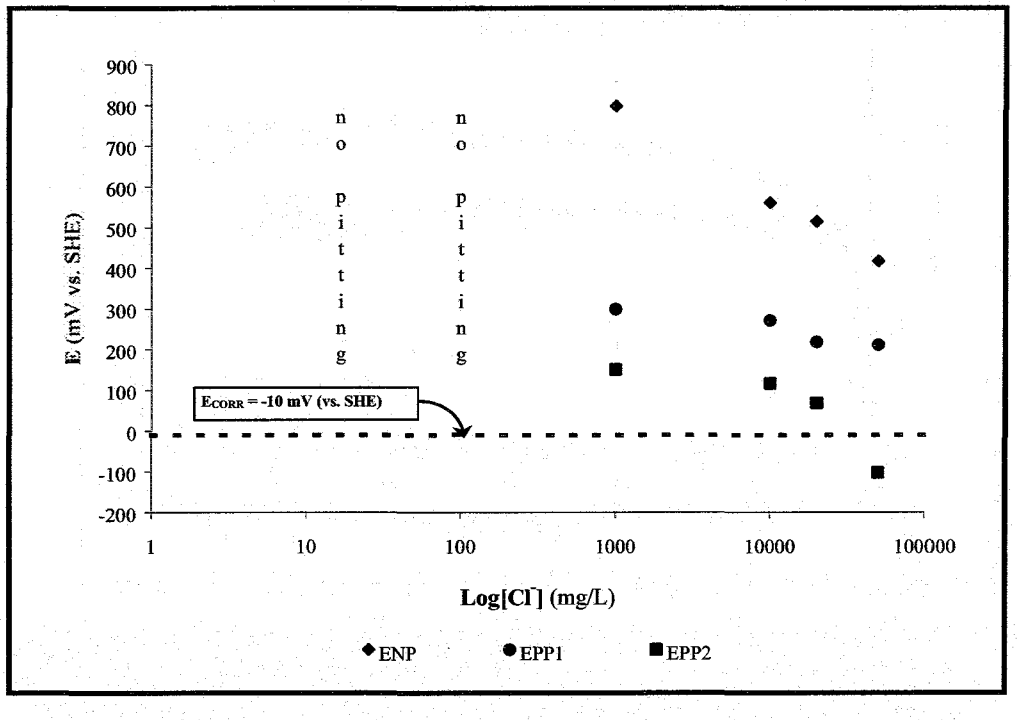

Figure 25: The characteristic pitting potentials (E_{NP}, E_{PP1}, and E_{PP2}) for stainless steel UHB 904L in SICW containing 0.2 mg/L SO_4^{2-} and varying Cl^-

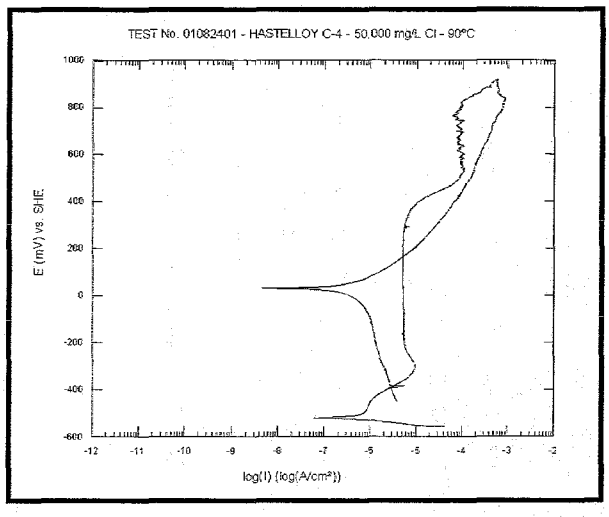

Figure 26: CPP-curve for HASTELLOY C-4 in SICW containing 0.2 mg/L SO_4^{2-} and 50,000 mg/L Cl^-.

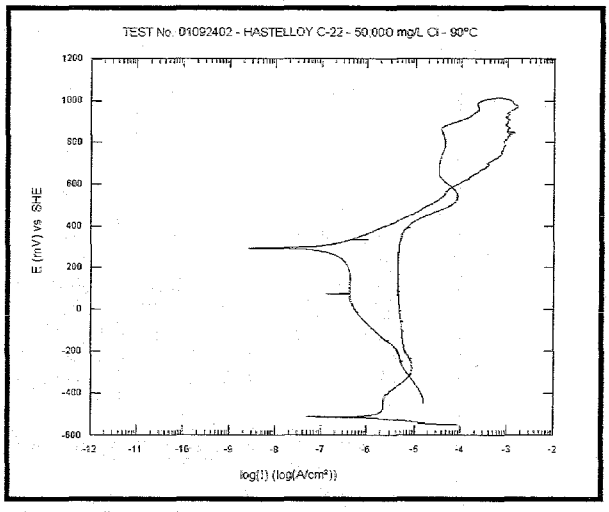

Figure 27: CPP-curve for HASTELLOY C-22 in SICW containing 0.2 mg/L SO_4^{2-} and 50,000 mg/L Cl^-.

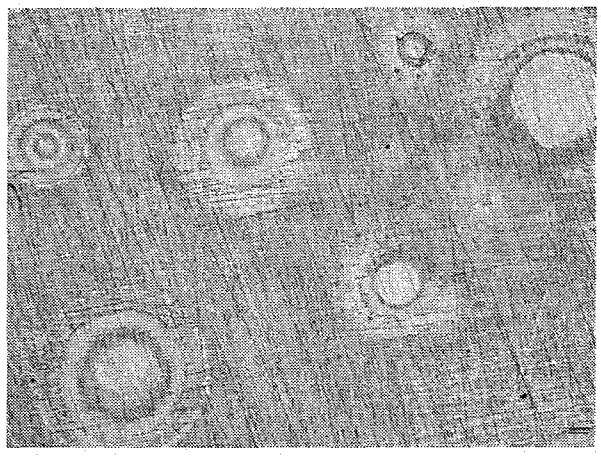

Figure 28:Optical micrograph of HASTELLOY C-4 after CPP-test in SICW containing 50,000 mg/L Cl^-, 50×

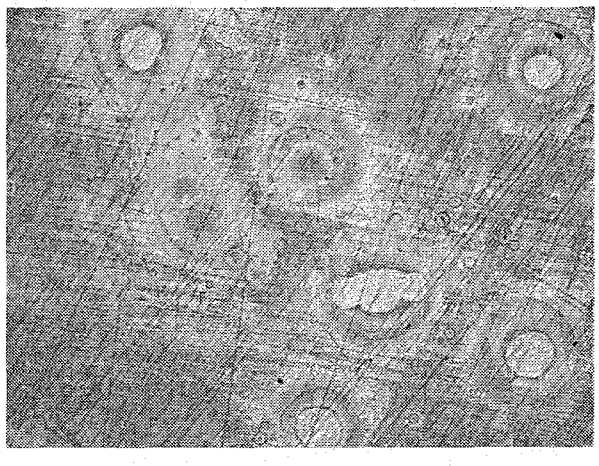

Figure 29:Optical micrograph of HASTELLOY C-22 after CPP-test in SICW containing 50,000 mg/L Cl^-, 50×

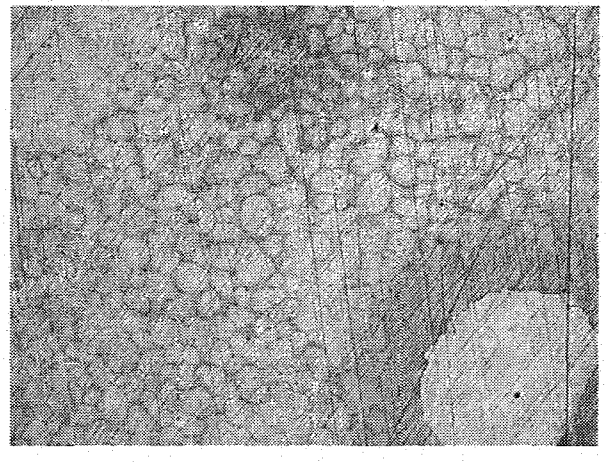

Figure 30:Optical micrograph of HASTELLOY C-22 after CPP-test in SICW containing 50,000 mg/L Cl^- with slight signs of IGA, 100×

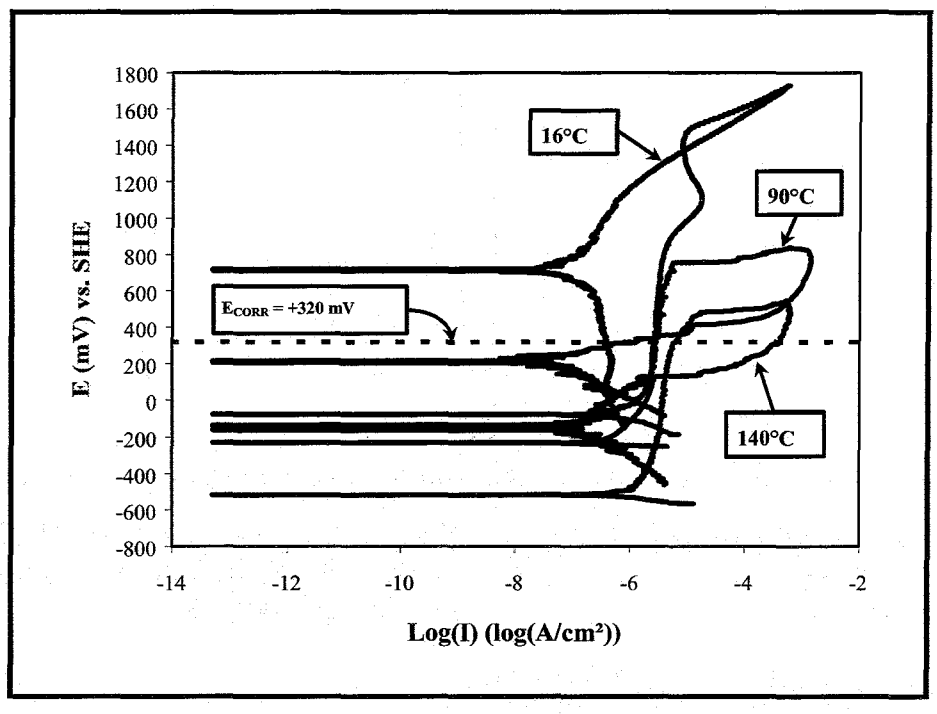

Figure 31: CPP-curves for stainless steel UHB 904L in SOCW containing 216 mg/L SO_4^{2-} and 1000 mg/L Cl^- at various temperatures.

ANNEX: Updated Time Schedule (Project: Container Corrosion Studies)

State: October 2001

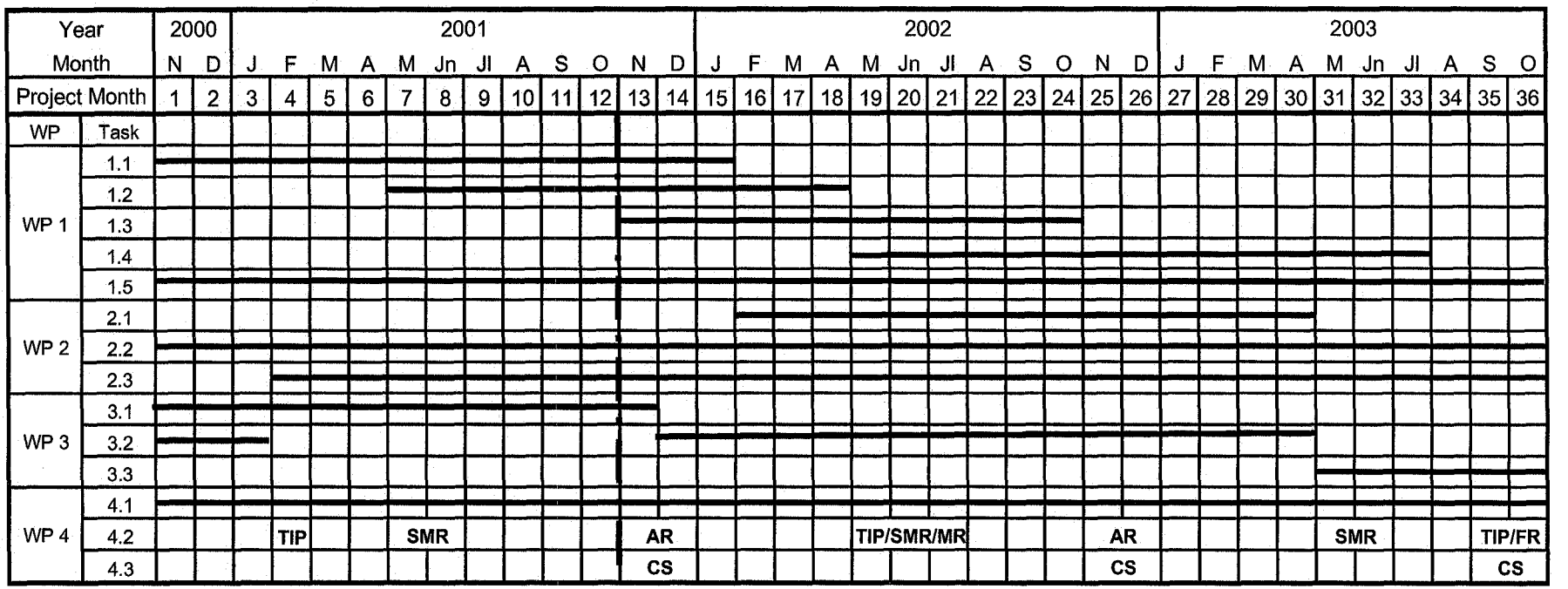

WP 1 : Salt environment
1.1 : Influence of thermal stress relief treatment on corrosion
1.2 : Contact corrosion between steel and Ti99.8-Pd
1.3 : Long-term corrosion studies on Cu-base materials
1.4 : Contact corrosion between steel and Cu-base materials
1.5 : Electrochemical corrosion studies

WP 2: Granitic environment
2.1 : Long-term corrosion studies on steel and Cu-base materials
2.2 : Stress corrosion cracking studies on Cu- and Ni-base materials
2.3 : Localized corrosion studies on Cu- and Ni-base materials

WP 3: Clay environment
3.1 : Influence of anaerobic conditions on corrosion
3.2 : Influence of elevated temperature on corrosion
3.3 : Influence of radiolysis products on corrosion

WP 4: Project management
4.1 : Co-ordination
4.2 : Reports
4.3 : Cost statements

TIP: Technolog. Implem. Plan
SMR: Six-months report
AR: Annual report
MR: Mid-term report
FR: Final report
CS: Cost statements

Time-Schedule-1.xls